

The Weak Neutral Current

Jens Erler¹ and Shufang Su²

¹Departamento de Física Teórica, Instituto de Física,
Universidad Nacional Autónoma de México, 04510 México D.F., México

²Department of Physics, University of Arizona,
P.O. Box 210081, Tucson, AZ 85721, USA

March 25, 2013

Abstract

This is a review of electroweak precision physics with particular emphasis on low-energy precision measurements in the neutral current sector of the electroweak theory and includes future experimental prospects and the theoretical challenges one faces to interpret these observables. Within the minimal Standard Model they serve as determinations of the weak mixing angle which are competitive with and complementary to those obtained near the Z -resonance. In the context of new physics beyond the Standard Model these measurements are crucial to discriminate between models and to reduce the allowed parameter space within a given model. We illustrate this for the minimal supersymmetric Standard Model with or without R -parity.

Contents

1	Introduction	2
2	The Standard Electroweak Theory	3
2.1	<i>Gauge sector and weak mixing angle</i>	3
2.2	<i>Higgs sector and the theory after electroweak symmetry breaking</i>	4
2.3	<i>Fermion sector and gauge currents</i>	6
3	Gauge and Higgs Boson Properties	7
3.1	<i>The effective leptonic weak mixing angle from the Z pole</i>	7
3.2	<i>The on-shell weak mixing angle from the W and Z boson masses</i>	10
3.3	<i>Implications for the Higgs boson mass</i>	12
3.4	<i>Implications for physics beyond the Standard Model</i>	15
4	Neutrino scattering	17
4.1	<i>Neutrino-electron scattering</i>	18
4.2	<i>Deep-inelastic neutrino-nucleus scattering and related processes</i>	19
4.3	<i>Radiative corrections</i>	23
5	Parity Violation	25
5.1	<i>Parity-violating Møller scattering</i>	25
5.2	<i>Parity non-conservation in atoms and ions</i>	26
5.3	<i>Parity-violating deep-inelastic scattering and related processes</i>	28
5.4	<i>Radiative corrections</i>	31
6	Constraints on Supersymmetry	33
6.1	<i>Minimal Supersymmetric Standard Model</i>	33
6.2	<i>R-parity conserving MSSM contributions to neutral current processes</i>	35
6.3	<i>R-parity violating supersymmetry</i>	36
7	Conclusions	38

1 Introduction

The basic structure of the Standard Model (SM) of the electroweak (EW) interactions was established in the 1970s with the help of low-energy (compared to the EW scale, $\Lambda_{\text{EW}} \equiv 246$ GeV) experiments in neutrino scattering and deep inelastic polarized electron-deuteron scattering, and later (after some initial confusion) in measurements of atomic parity violation (APV). The 1980s saw the first precision measurements of the EW mixing angle in neutrino scattering and charged lepton scattering in various kinematic regimes. The Z-pole programs at LEP 1 and the SLC with their high-precision measurements of Z boson properties finally established the SM as the correct theory even at the level of small quantum corrections. This permits to view the SM as the low energy effective theory of a more fundamental theory with a typical energy scale in the TeV or multi-TeV domain (or conceivably much higher). The current energy frontier at the Large Hadron Collider (LHC) directly probes this regime by looking for new particles or strong deviations from the SM predictions of cross-sections and event rates.

However, there is an important alternative route. One can return to the sub-Z-pole regime attaining high precision by performing ultra-high statistics experiments at the so-called intensity frontier [1]. By either using neutrinos or by exploiting the parity-violating nature of the weak interaction one is directly

sensitive to Λ_{EW} , so that a measurement of about 1% precision generally probes the multi TeV energy scale. Cases in which the SM prediction happens to be suppressed are even more favorable. This class of measurements and the associated theoretical challenges are the main subject of this review. Cases where the SM prediction is even vanishing due to an accidental symmetry such as lepton number or lepton flavor number, and observables where it is tiny because they violate some approximate discrete symmetries like time reversal are covered elsewhere in this volume. For a previous review discussing low energy neutral current measurements we refer to Ref. [2]. The most recent review [3] covers the weak mixing angle at low momentum transfer and parity-violating electron scattering. It also contains a detailed documentation of the theory issues surrounding the weak charge of the proton and the scale dependence of the weak mixing angle, as well as a discussion of new physics, such as contact interactions, extra neutral Z bosons (both visible and dark) and the X parameter (see Section 3.4).

It is difficult to overemphasize the complementarity between the energy and intensity frontiers. Measurements of the W and Z boson properties have reached and surpassed per mille precision but they may be insensitive to new physics, if mixing and interference effects are too small. New particles can be produced at the LHC, but only if they are either light enough, or couple sufficiently strong to quarks and gluons, or allow a clean final state (preferentially involving charged leptons or photons). By contrast, lower energy observables are affected by amplitudes mediated by new physics, even if they are hiding below the Z resonance where they might be out of phase. Also, measurements of EW couplings of the first generation quarks are very difficult at the energy frontier, a gap that is naturally closed by the intensity frontier.

Of course, the indirect nature of the precision measurements from the intensity frontier makes it virtually impossible to identify the type of new physics responsible for a possible deviation from the SM. However, by having at one's disposal a whole array of measurements of comparable precision reintroduces some discriminatory power, and comparison with the discoveries (or lack thereof) at the energy frontier strengthens this point further.

This report is structured as follows: Section 2 summarizes the salient features of the SM¹. In Section 3 we review the very high-precision measurements of various properties of the massive gauge bosons and their implications for the mass of the SM Higgs boson. In Section 4 we turn to the intensity frontier and discuss neutrino scattering experiments. Section 5 is dedicated to polarized lepton scattering and atomic parity violation. As a specific scenario for physics beyond the SM, section 6 discusses models of supersymmetry which are very well motivated from a theoretical point of view. Section 7 concludes with a summary and an outlook.

2 The Standard Electroweak Theory

2.1 Gauge sector and weak mixing angle

Any relativistic quantum field theory which contains as mediators massless particles of helicity ± 1 and which in turn are described in terms of vector fields, V_μ (necessary on dimensional grounds if one wants to avoid extra power suppressions by some large mass scale), is subject to a set of exact gauge symmetries [5]. The electroweak SM [6] is based on the gauge group $SU(2)_L \times U(1)_Y$ [7] with corresponding vector fields W_μ^i ($i = 1, 2, 3$) and B_μ , where $SU(2)_L$ refers to weak isospin and Y denotes hypercharge. In terms of the $SU(2)_L$ and $U(1)_Y$ gauge couplings, g and g' , and the weak mixing angle, θ_W , the linear combinations,

$$W_\mu^\pm \equiv \frac{W_\mu^1 \mp iW_\mu^2}{\sqrt{2}}, \quad Z_\mu \equiv \frac{gW_\mu^3 - g'B_\mu}{\sqrt{g^2 + g'^2}} \equiv \cos \theta_W W_\mu^3 - \sin \theta_W B_\mu, \quad (1)$$

¹For a recent and much more detailed treatment, see *e.g.*, Ref. [4].

$$A_\mu \equiv \frac{g'W_\mu^3 + gB_\mu}{\sqrt{g^2 + g'^2}} \equiv \sin \theta_W W_\mu^3 + \cos \theta_W B_\mu, \quad (2)$$

give rise to the charged and neutral gauge bosons of the weak interaction, and the photon, respectively. These vector fields enter the SM Lagrangian,

$$\mathcal{L} = \mathcal{L}_V + \mathcal{L}_\phi + \mathcal{L}_f + \mathcal{L}_Y, \quad (3)$$

through the kinetic terms for the vector gauge fields,

$$\mathcal{L}_V = -\frac{1}{4}W^{\mu\nu i}W_{\mu\nu}^i - \frac{1}{4}B^{\mu\nu}B_{\mu\nu}, \quad (4)$$

where

$$W_{\mu\nu}^i = \partial_\mu W_\nu^i - \partial_\nu W_\mu^i - g\epsilon_{ijk}W_\mu^jW_\nu^k, \quad B_{\mu\nu} = \partial_\mu B_\nu - \partial_\nu B_\mu, \quad (5)$$

and through the gauge covariant derivatives in \mathcal{L}_ϕ and \mathcal{L}_f discussed in Sections 2.2 and 2.3, respectively.

2.2 Higgs sector and the theory after electroweak symmetry breaking

In the minimal model, EW symmetry breaking is introduced with the help of a weak iso-doublet, ϕ [8], of complex scalars, with Lagrangian density,

$$\mathcal{L}_\phi = (D^\mu \phi)^\dagger D_\mu \phi - \mu^2 \phi^\dagger \phi - \frac{\lambda^2}{2}(\phi^\dagger \phi)^2 \equiv (D^\mu \phi)^\dagger D_\mu \phi - V(\phi), \quad (6)$$

where $\lambda^2 > 0$ is required for a stable vacuum, and where $\mu^2 < 0$ triggers the spontaneous breaking of the EW gauge symmetry [9–12]. The Lagrangian (6) is easily seen to have an $SO(4) \simeq SU(2) \times SU(2)$ global (“custodial”) symmetry which is, however, broken down to $SU(2)_L \times U(1)_Y$ by the gauge and Yukawa interactions. The gauge covariant derivative of ϕ is,

$$D_\mu \phi = (\partial_\mu + igT_i^\phi W_\mu^i + ig'Y^\phi B_\mu)\phi = \left[\partial_\mu + i\frac{g}{\sqrt{2}}(T_+^\phi W_\mu^+ + T_-^\phi W_\mu^- + Q_A^\phi A_\mu + g^\phi Z_\mu) \right] \phi, \quad (7)$$

with weak isospin and hypercharge generators given, respectively, in terms of the Pauli matrices, τ_i , and the identity matrix, $\tau_0 \equiv \mathbb{I}_2$, by,

$$T_i^\phi = \frac{\tau_i}{2}, \quad Y^\phi = \frac{\tau_0}{2}. \quad (8)$$

For later reference we introduced a common normalization for the generators of all four EW gauge bosons in the second form in Eq. (7), for which we defined,

$$T_\pm^\phi \equiv T_1^\phi \pm iT_2^\phi = T_\mp^{\phi\dagger}, \quad Q_A^\phi \equiv \sqrt{2} \sin \theta_W (T_3^\phi + Y^\phi) \equiv \sqrt{2} \sin \theta_W Q^\phi = Q_A^{\phi\dagger}, \quad (9)$$

$$g^\phi \equiv \sqrt{2} \cos \theta_W (T_3^\phi - \tan^2 \theta_W Y^\phi) = \frac{\sqrt{2} T_3^\phi - \sin \theta_W Q_A^\phi}{\cos \theta_W} = \sqrt{2} \frac{T_3^\phi - \sin^2 \theta_W Q^\phi}{\cos \theta_W} = g^{\phi\dagger}, \quad (10)$$

and where Q^ϕ is the electric charge operator normalized in the usual way². Note the similarity in the relations for T_\pm^ϕ , Q_A^ϕ , and g^ϕ , in the ideal mixing case $g = g'$ ($\tan \theta_W = 1$) where we also have $Q_A^\phi = Q^\phi$.

²All the explicit factors of $\sqrt{2}$ appearing in Q_A^ϕ , g^ϕ , and Eq. (7) are an artifact of the normalization used in the physics literature for the gauge symmetry generators. They would be absent in the more natural normalization typically used by mathematicians in which, *e.g.*, all Dynkin indices are integers.

Since one wants to quantize the theory around the classical vacuum, the physically relevant case, $\mu^2 < 0$, requires a redefinition of the original Higgs field, ϕ , so that at the minimum of the potential all fields have vanishing vacuum expectation values (VEVs),

$$\phi \equiv \frac{1}{\sqrt{2}} \begin{pmatrix} \phi_1 + i\phi_2 \\ \phi_3 + i\phi_4 \end{pmatrix} = \frac{1}{\sqrt{2}} \begin{pmatrix} \phi_1 + i\phi_2 \\ H + v + i\phi_4 \end{pmatrix} \Rightarrow \langle \phi \rangle = \frac{1}{\sqrt{2}} \begin{pmatrix} 0 \\ v \end{pmatrix}. \quad (11)$$

The three VEVs, $\langle \phi_i \rangle$ for $i = 1, 2, 4$, have been arranged to vanish by a global $SU(2)_L \times U(1)_Y$ transformation, while for $\langle \phi_3 \rangle = v$ one defines the physical Higgs field, $H \equiv \phi_3 - v$, so that $\langle H \rangle = 0$. The potential, $V(\phi)$, now gives rise to three massless and non-interacting scalars, which in the absence of the gauge fields would be Goldstone bosons [13]. By performing a local $SU(2)_L \times U(1)_Y$ transformation one can finally proceed to the unitary gauge in which these three bosons disappear from the physical spectrum and instead provide the longitudinal components of the W and Z bosons. It remains one massive scalar mode, the physical Higgs boson. The terms quadratic in v arising from \mathcal{L} in Eq. (6) are,

$$\frac{v^2}{2} \left[\lambda^2 H^2 + \frac{g^2}{2} (W^{\mu-} W_{\mu}^+ + (g^{\phi})^2 Z^{\mu} Z_{\mu}) \right],$$

so that

$$M_H = \lambda v = \sqrt{-2\mu^2}, \quad M_W = \frac{g}{2}v, \quad M_Z = \frac{M_W}{\cos \theta_W} = \frac{\sqrt{g^2 + g'^2}}{2}v. \quad (12)$$

The value of $v = 246.22$ GeV is fixed by the Fermi constant,

$$G_F = 1.1663787(6) \times 10^{-5} \text{ GeV}^{-2} = \frac{1}{\sqrt{2}v^2}, \quad (13)$$

and G_F itself can be cleanly extracted from the μ lifetime, τ_{μ} , which was measured recently by the MuLan Collaboration at the PSI with an order of magnitude improved precision, $\tau_{\mu} = 2.1969803(22) \mu\text{s}$ [14].

Thus, at lowest order one can write,

$$\sin^2 \theta_W = 1 - \frac{M_W^2}{M_Z^2} = \frac{g'^2}{g^2 + g'^2}, \quad (14)$$

and one may elevate either form to an exact definition of $\sin^2 \theta_W$ to all orders in perturbation theory. The first relation defines the on-shell renormalization scheme, and is manifestly related directly to physically observable particles masses³. The second, coupling-based relation leads to theoretical constructs which depend on details of the regularization scheme, the energy scale (μ), the treatment of fermion thresholds, *etc.* This class includes the $\overline{\text{MS}}$ -scheme definition, $\sin^2 \hat{\theta}_W(\mu)$, and a variant used in supersymmetric theories, which is based on the $\overline{\text{DR}}$ -scheme. These definitions have the advantages that they significantly simplify higher-order calculations, and the numerical values of different couplings can be directly compared as, *e.g.*, in the discussion of gauge coupling unification. Moreover, the large Yukawa coupling of the top quark, Y_t , and relatedly its heavy mass, $m_t = Y_t v$, strongly affect the renormalized value of M_W , while its effect on M_Z and $\sin^2 \hat{\theta}_W(\mu)$ is much weaker. Therefore, using the on-shell definition indiscriminately may distort theoretical expressions and lead to a poorer convergences of the perturbative series. Further definitions and more details can be found in Ref. [15].

The scale dependence of the weak mixing angle renormalized in the $\overline{\text{MS}}$ -scheme [17] is shown in Figure 1. The minimum of the curve corresponds to $Q = M_W$, below which we switch to an effective theory with the W^{\pm} bosons integrated out, and where the β -function for the weak mixing angle changes sign. For the scale dependence in a mass-dependent renormalization scheme, see Ref. [18], and for a recent review on the low energy measurements of the weak mixing angle, see also Ref. [3].

³We note, however, that at higher orders the definition of the mass of an unstable particle becomes ambiguous, and the whole concept of observability becomes demoted.

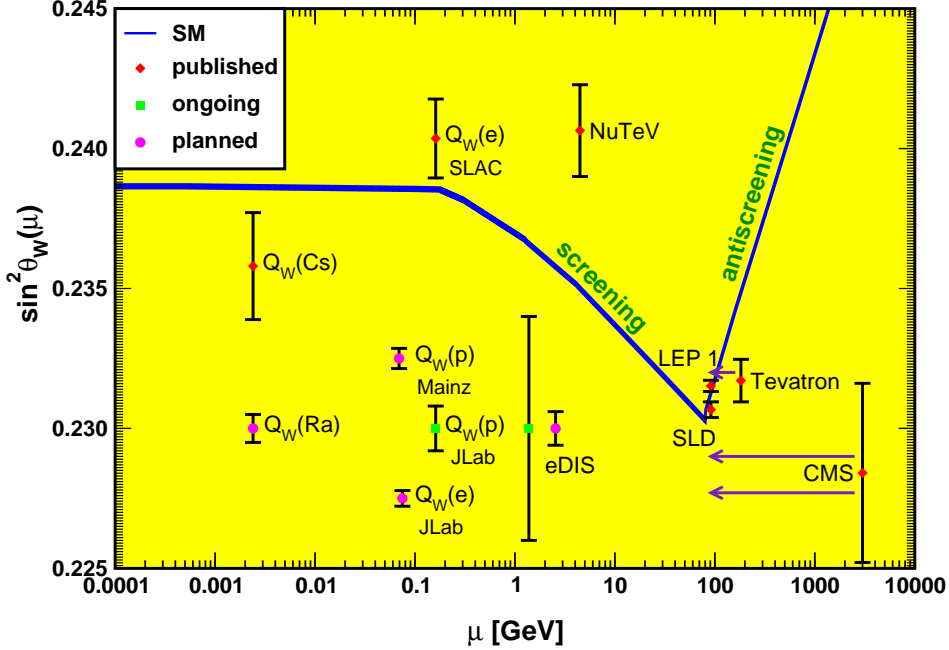


Figure 1: Scale dependence of the weak mixing angle in the $\overline{\text{MS}}$ -scheme. At the location of M_W and each fermion mass there are discontinuities arising from scheme dependent matching terms which are necessary to ensure that the various effective field theories within a given loop order describe the same physics. However, in the $\overline{\text{MS}}$ -scheme these are very small numerically and barely visible in the figure provided one decouples quarks at $\mu = \hat{m}_q(\hat{m}_q)$. The width of the curve reflects the theory uncertainty from strong interaction effects which at low energies is at the level of $\pm 7 \times 10^{-5}$ [17]. The various data points are discussed in the subsequent sections. The Tevatron and CMS measurements are strongly dominated by invariant masses of the final state dilepton pair of $\mathcal{O}(M_Z)$ and can thus be considered as additional Z -pole data points, but for clarity we shifted the points horizontally to the right.

2.3 Fermion sector and gauge currents

At the renormalizable level, *i.e.*, ignoring, for example, the possibility of Majorana neutrino masses and other lepton or baryon number violating effects⁴, the parts of \mathcal{L} containing fermions are given by,

$$\mathcal{L}_f = i \sum_{m=1}^3 [\bar{Q}_m \not{D} Q_m + \bar{L}_m \not{D} L_m + \bar{U}_m \not{D} U_m + \bar{D}_m \not{D} D_m + \bar{E}_m \not{D} E_m], \quad (15)$$

$$\mathcal{L}_Y = -\sqrt{2} \sum_{m,n=1}^3 [Y_{mn}^u (i\tau_2 \phi^\dagger) \bar{Q}_m U_n + Y_{mn}^d \phi \bar{Q}_m D_n + Y_{mn}^e \phi \bar{L}_m E_n] + \text{H.c.}, \quad (16)$$

⁴Majorana neutrino masses from dimension 5 operators [19] and their implications for neutrino oscillations and neutrinoless double beta decay are covered elsewhere in this volume.

where the covariant derivatives are defined in analogy to Eq. (7) and the sums are over fermion families. The relations (9) and (10) are general and apply to fermions, as well. Left-handed fermions, $\psi_L \equiv P_L \psi$, form the iso-doublets $\mathbf{L} \equiv (\nu_L, e_L^-)^T$ and $\mathbf{Q} \equiv (u_L, d_L)^T$, while right-handed fermions, $\psi_R \equiv P_R \psi$, are iso-singlets denoted by $\mathbf{E} \equiv e_R$, $\mathbf{U} \equiv u_R$, and $\mathbf{D} \equiv d_R$, and so in summary,

$$P_{L/R} \equiv \frac{1 \mp \gamma^5}{2}, \quad T_L^i = \frac{\tau^i}{2}, \quad T_R^i = 0, \quad Y_f = Q_f - T_f^3. \quad (17)$$

The Y_{mn}^f ($f = e, u, d$) are arbitrary complex 3×3 Yukawa matrices. After symmetry breaking one finds,

$$\mathcal{L}_f + \mathcal{L}_Y = \sum_r \bar{\psi}_r \left[i \not{\partial} - m_r \left(1 + \frac{H}{v} \right) \psi_r \right] - \frac{g}{\sqrt{2}} \left[J_W^\mu \dagger W_\mu^+ + J_W^\mu W_\mu^- + J_A^\mu A_\mu + J_Z^\mu Z_\mu \right], \quad (18)$$

where r is a double index running over m and $f = \nu, e, u, d$, and where the charged, electromagnetic and weak neutral currents are given by,

$$J_W^\mu = \sum_{m=1}^3 \left[\bar{d}_m \gamma^\mu V_{CKM}^\dagger P_L u_m + \bar{e}_m \gamma^\mu P_L \nu_m \right], \quad (19)$$

$$J_A^\mu = \sqrt{2} \sin \theta_W \sum_{m=1}^3 \left[\frac{2}{3} \bar{u}_m \gamma^\mu u_m - \frac{1}{3} \bar{d}_m \gamma^\mu d_m - \bar{e}_m \gamma^\mu e_m \right], \quad (20)$$

$$J_Z^\mu = \sum_f \bar{\psi}_f \gamma^\mu \left[g_L^f P_L + g_R^f P_R \right] \psi_f = \sum_f \bar{\psi}_f \gamma^\mu \frac{g_V^f - g_A^f \gamma^5}{2} \psi_f = \quad (21)$$

$$\frac{1}{\sqrt{2} \cos \theta_W} \sum_{m=1}^3 \left[\bar{u}_m \gamma^\mu P_L u_m - \bar{d}_m \gamma^\mu P_L d_m + \bar{\nu}_m \gamma^\mu P_L \nu_m - \bar{e}_m \gamma^\mu P_L e_m \right] - \tan \theta_W J_A^\mu. \quad (22)$$

The matrix $V_{CKM} \equiv A_L^{u\dagger} A_L^d$ has entered into J_μ^W after unitary field re-definitions,

$$u_L \rightarrow A_L^u u_L, \quad u_R \rightarrow A_R^u u_R, \quad d_L \rightarrow A_L^d d_L, \quad d_R \rightarrow A_R^d u_R, \quad (23)$$

have been applied in order to write Eq. (18) in terms of mass eigenstates. We also defined vector and axial-vector Z couplings as,

$$g_V^f \equiv g_L^f + g_R^f = \sqrt{2} \frac{T_f^3 - 2 \sin^2 \theta_W Q_f}{\cos \theta_W}, \quad g_A^f \equiv g_L^f - g_R^f = \sqrt{2} \frac{T_f^3}{\cos \theta_W}. \quad (24)$$

At low energies, $Q^2 \equiv -q^2 \ll M_{W,Z}^2$, one finds the effective four-fermion interactions,

$$\mathcal{L}_{CC} = -\frac{2}{v^2} J_W^{\mu\dagger} J_{W\mu}, \quad \mathcal{L}_{NC} = -\frac{\cos^2 \theta_W}{v^2} J_Z^\mu J_{Z\mu}. \quad (25)$$

3 Gauge and Higgs Boson Properties

3.1 The effective leptonic weak mixing angle from the Z pole

The most precise determinations of the weak mixing angle to date have been obtained at the e^+e^- -annihilation Z factories, LEP and SLC, from measurements of various Z -pole asymmetries in which systematic uncertainties largely cancel. After correcting for QED (including photon s -channel exchange), interference and the tiny box graph effects, and where applicable for QCD or t -channel γ and

Z exchanges, and after extrapolating to $\sqrt{s} = M_Z$ and ideal beam polarizations (0 or 100%), these asymmetries can be expressed in terms of the physics parameters,

$$A^f \equiv \frac{2g_V^f g_A^f}{(g_V^f)^2 + (g_A^f)^2}. \quad (26)$$

In particular, the electron beam at the SLC was longitudinally polarized, where the luminosity-weighted average degree of polarization, P^e , was about 75%. The small polarimetry error of 0.5% permitted the SLD Collaboration to measure the polarization or left-right asymmetry into hadronic final states [20],

$$A_{LR}^q \equiv \frac{\sigma_L - \sigma_R}{\sigma_L + \sigma_R} = A^e = \frac{1 - 4 \sin^2 \theta_{\text{eff}}^\ell}{1 - 4 \sin^2 \theta_{\text{eff}}^\ell + 8 \sin^4 \theta_{\text{eff}}^\ell}, \quad (27)$$

with high precision, where σ_L (σ_R) is the cross-section for left (right)-handed polarized electrons. $\sin^2 \theta_{\text{eff}}^\ell$ is the effective Z pole weak mixing angle entering the vector coupling for charged leptons⁵. Thus it constitutes a coupling-based definition and is numerically close to the value in the $\overline{\text{MS}}$ -scheme,

$$\sin^2 \theta_{\text{eff}}^\ell \equiv \frac{1}{4} \left[1 - \frac{g_V^\ell}{g_A^\ell} \right] = \sin^2 \hat{\theta}_W(M_Z) + 0.00029. \quad (28)$$

As indicated in Eq. (27), the initial state polarization asymmetry filters out the initial state coupling, A^e , regardless of the final state. This is advantageous because on the one hand A^e is proportional to $1 - 4 \sin^2 \theta_{\text{eff}}^\ell$, and on the other hand $\sin^2 \theta_{\text{eff}}^\ell$ is numerically close to 1/4, which results in very high sensitivity to $\sin^2 \theta_{\text{eff}}^\ell$. SLD was able to extract the final-state couplings A^b , A^c [21], A^s [22], A^τ and A^μ [23] from combined left-right, forward-backward asymmetries, using

$$A_{LR,FB}^f = \frac{\sigma_{LF}^f - \sigma_{LB}^f - \sigma_{RF}^f + \sigma_{RB}^f}{\sigma_{LF}^f + \sigma_{LB}^f + \sigma_{RF}^f + \sigma_{RB}^f} = \frac{3}{4} A^f, \quad (29)$$

where, for example, σ_{LF}^f is the cross-section for left-handed polarized incident electrons to produce a fermion f traveling in the forward hemisphere. Polarized Bhabba scattering represents mostly a measurement of A_{LR}^ℓ but it also includes information about $A_{LR,FB}^\ell$, both of which providing the parameter A_e [23]. A^e is also proportional to the hadronic asymmetry ratio formed by the forward-backward charge asymmetry, A_{FB}^q , normalized to the left-right forward-backward charge asymmetry, $A_{LR,FB}^q$ [24].

LEP was not operating with polarized beams, but A^τ was measured by the LEP 1 Collaborations (ALEPH, DELPHI, L3 and OPAL \equiv ADLO) [21] through the total final state τ polarization, \mathcal{P}^τ , and A^e was extracted from its angular distribution or forward-backward asymmetry,

$$\mathcal{P}^\tau = -A^\tau, \quad \mathcal{P}_{FB}^\tau = -\frac{3}{4} A^e. \quad (30)$$

The Z -pole forward-backward asymmetries at LEP 1 are given by

$$A_{FB}^f = \frac{3}{4} A^e A^f, \quad (31)$$

where $f = e, \mu, \tau, b, c, s$ [25] and q , and where as before A_{FB}^q refers to the hadronic charge asymmetry.

As for hadron colliders, the forward-backward asymmetry, A_{FB} , for e^+e^- final states (with invariant masses restricted to or dominated by values around M_Z) in $p\bar{p}$ collisions has been measured by the DØ [26] and CDF [27] Collaborations at the Tevatron and values for the weak mixing angle were extracted, which combine to $\sin^2 \theta_{\text{eff}}^e = 0.2320 \pm 0.0008$ (assuming common PDF uncertainties).

⁵We use the symbol ℓ for a generic charged lepton when lepton universality is assumed.

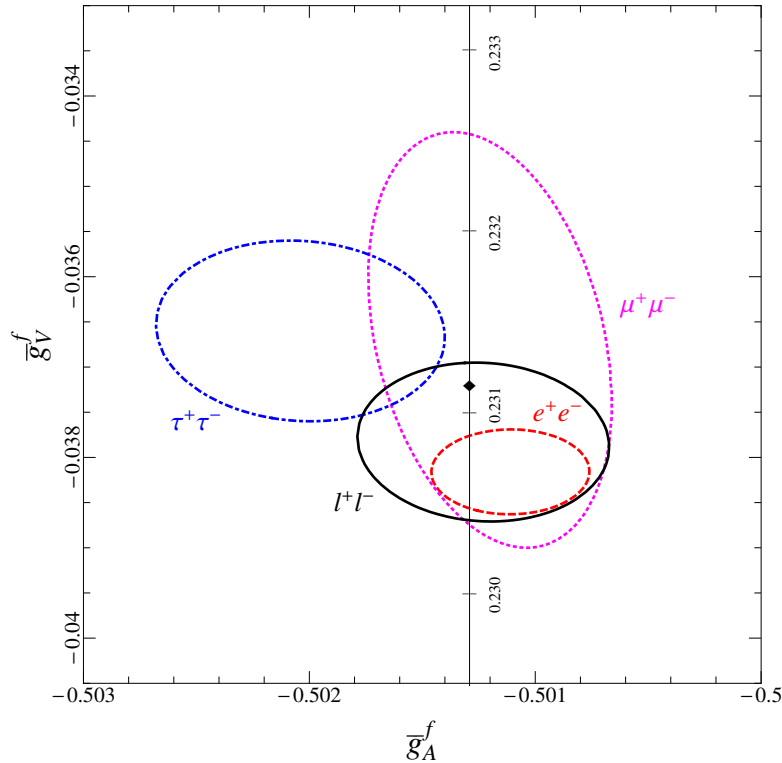


Figure 2: 1σ (39.35% CL) regions for the Z -pole observables \bar{g}_V^f and \bar{g}_A^f , $f = e, \mu, \tau$, obtained at LEP and the SLC [21], compared to the SM expectation as a function of $\sin^2 \hat{\theta}_W(M_Z)$ with the SM best fit value, $\sin^2 \hat{\theta}_W(M_Z) = 0.23116$, indicated. Also shown is the 90% CL contour in $\bar{g}_{A,V}^\ell$ obtained assuming lepton universality. (Figure reprinted as permitted according to journal guidelines from *Phys. Rev. D* 86 (2012) 010001, J. Erler and P. Langacker [15].)

This kind of measurement is harder in the pp environment due to the difficulty to assign the initial quark and antiquark in the underlying Drell-Yan process to the protons. Nevertheless, the CMS Collaboration [28] at the LHC was able to report a measurement of $\sin^2 \theta_{\text{eff}}^\mu$ from their dimuon data based on an integrated luminosity of 1.1 fb^{-1} . Given that the event sample size will grow by several orders of magnitude, and further results can be anticipated from e^+e^- final states, as well as from the ATLAS Collaboration, there is the potential of much more precise determinations of $\sin^2 \theta_{\text{eff}}^\ell$ from the LHC.

The LEP and SLC asymmetries and branching ratios can also be analyzed in terms of model-independent couplings, \bar{g}_V^f and \bar{g}_A^f , where the bar indicates a different normalization and the inclusion of radiative corrections [29]. Their SM values can be obtained by multiplying Eqs. (24) by $\sqrt{2\rho_f} \cos \theta_W$, where $\rho_f \neq 1$ is a radiative correction parameter, and by employing $\sin^2 \theta_{\text{eff}}^f$ in g_V^f . The resulting \bar{g}_V^f and \bar{g}_A^f for $f = e, \mu, \tau$ and ℓ are shown in Figure 2.

Table 1 summarizes the Z -pole asymmetry measurements with enhanced sensitivity to $\sin^2 \theta_{\text{eff}}^\ell$ and the corresponding extractions. Notice, that there is a 3.1σ discrepancy between the two most precise determinations, namely A_{LR}^q from the SLC and A_{FB}^b from LEP. On the other hand, the average of all measurements coincides exactly with the SM prediction for $M_H = 125 \text{ GeV}$. Note also, that all other measurements, *i.e.*, excluding A_{LR}^q and A_{FB}^b , average to $\sin^2 \theta_{\text{eff}}^\ell = 0.23153 \pm 0.00025$, which is also in perfect agreement with the SM prediction for $M_H = 125 \text{ GeV}$. This may be an indication that the 2.2σ deviations in A_{LR}^q and A_{FB}^b might be due to fluctuations in opposite directions from the SM. Also, the $Z \rightarrow b\bar{b}$ partial decay width normalized to the total hadronic width, R^b , and other analogously defined

Table 1: Z -pole asymmetry measurements from the high-energy frontier (CERN, SLAC and FNAL) compared to the SM predictions for $M_H = 125$ GeV. The corresponding effective weak mixing angles, $\sin^2 \theta_{\text{eff}}^\ell$, and pulls (in standard deviations) from the SM prediction, $\sin^2 \theta_{\text{eff}}^\ell = 0.23158$ (for $M_H = 125$ GeV), are shown in the last two columns, respectively. Note, that the theory (PDF) uncertainty entering the CDF result [27] is adjusted to coincide and treated as fully correlated with the corresponding DØ result [26]. The total average in the last line accounts for further correlations [21] between various individual measurements.

Group(s)	collider	Ref.	asymmetry	measurement	SM	$\sin^2 \theta_{\text{eff}}^\ell$	deviation
SLD	SLC	[20]	A_{LR}^q	0.1514 ± 0.0022	0.1466	0.23097 ∓ 0.00027	−2.2
SLD	SLC	[23]	A_{LR}^ℓ	0.1544 ± 0.0060	0.1466	0.23058 ∓ 0.00076	−1.3
SLD	SLC	[23]	$A_{LR,FB}^\mu$	0.142 ± 0.015	0.1466	0.2322 ∓ 0.0019	+0.3
SLD	SLC	[23]	$A_{LR,FB}^\tau$	0.136 ± 0.015	0.1466	0.2329 ∓ 0.0019	+0.7
SLD	SLC	[24]	A^e	0.162 ± 0.043	0.1466	0.2296 ∓ 0.0055	−0.4
ADLO	LEP 1	[21]	A_{FB}^b	0.0992 ± 0.0016	0.1028	0.23221 ∓ 0.00029	+2.2
ADLO	LEP 1	[21]	A_{FB}^c	0.0707 ± 0.0035	0.0734	0.23220 ∓ 0.00081	+0.8
ADLO	LEP 1	[22]	A_{FB}^s	0.0976 ± 0.0114	0.1029	0.2325 ∓ 0.0021	+0.4
ADLO	LEP 1	[21]	A_{FB}^q	0.0403 ± 0.0026	0.0421	0.2324 ∓ 0.0012	+0.7
ADLO	LEP 1	[21]	A_{FB}^e	0.0145 ± 0.0025	0.0161	0.2325 ∓ 0.0015	+0.6
ADLO	LEP 1	[21]	A_{FB}^μ	0.0169 ± 0.0013	0.0161	0.23113 ∓ 0.00073	−0.6
ADLO	LEP 1	[21]	A_{FB}^τ	0.0188 ± 0.0017	0.0161	0.23008 ∓ 0.00091	−1.6
ADLO	LEP 1	[21]	$-\mathcal{P}^\tau$	0.1439 ± 0.0043	0.0161	0.23192 ∓ 0.00055	+0.6
ADLO	LEP 1	[21]	$-4/3 \mathcal{P}_{FB}^\tau$	0.1498 ± 0.0049	0.0161	0.23117 ∓ 0.00062	−0.7
DØ	Tevatron	[26]	$\sin^2 \theta_{\text{eff}}^e$			0.2309 ± 0.0010	−0.7
CDF	Tevatron	[27]	$\sin^2 \theta_{\text{eff}}^e$			0.2329 ± 0.0009	+1.4
CMS	LHC	[28]	$\sin^2 \theta_{\text{eff}}^\mu$			0.2287 ± 0.0032	−0.9
all	all		$\sin^2 \theta_{\text{eff}}^\ell$			0.23155 ± 0.00016	−0.2

R^q , are generally in reasonable agreement with the SM. This makes it difficult to construct plausible new physics models which would shift A_{FB}^b away from its SM value by modifying the A^b factor in Eq. (31). There is, however, a very recent fermionic two-loop calculation [31] of R^b , which shifts the SM prediction about 2.3 below the experimental value. This is an interesting development but it should be cautioned that the contribution of purely bosonic loops at this order is still unknown. Also, even if confirmed, the new physics effects proportional to $\sin^2 \theta_{\text{eff}}^b$ would have to be an order of magnitude larger than contributions to ρ_b , so there would likely be some tuning.

3.2 The on-shell weak mixing angle from the W and Z boson masses

As discussed in Section 2.2, the weak mixing angle can also be derived directly from the W and Z boson masses. The Z -lineshape scan at LEP 1 [21] produced a determination of M_Z of ultra-high precision,

$$M_Z = 91.1876 \pm 0.0021 \text{ GeV}. \quad (32)$$

Table 2: W -boson mass measurements from the high-energy frontier (CERN and FNAL) to be compared with the SM prediction, $M_W = 80.369$ GeV (for $M_H = 125$ GeV). The corresponding on-shell weak mixing angles, s_W^2 , from the combination with M_Z , and pulls (in standard deviations) from the SM prediction, $s_W^2 = 0.22320$ (for $M_H = 125$ GeV), are shown in the last two columns, respectively.

Group(s)	collider	Ref.	M_W [GeV]	$s_W^2 \equiv 1 - \frac{M_W^2}{M_Z^2}$	deviation
ADLO	LEP 2	[32]	80.376 ± 0.033	0.22307 ∓ 0.00064	-0.2
CDF & DØ	Tevatron	[33]	80.387 ± 0.016	0.22286 ∓ 0.00031	-1.1
all	both		80.385 ± 0.015	0.22290 ∓ 0.00028	-1.1

Precise values for M_W were obtained in W -pair production at LEP 2 [32] and single- W production at the Tevatron [33]. They are shown in Table 2 together with the corresponding values for the weak mixing angle in the on-shell scheme, $s_W^2 = 1 - c_W^2$, computed using Eq. (32).

The error in the world average of s_W^2 in Table 2 is significantly larger than the corresponding error in $\sin^2 \theta_{\text{eff}}^\ell$ in Table 1. However, a fairer comparison would be based on the quantities defined in Eqs. (12) and (14) which we relate in various ways to G_F and the fine structure constant, α , through,

$$M_W \sqrt{1 - \frac{M_W^2}{M_Z^2}} = M_W \sin \theta_W = M_Z \cos \theta_W \sin \theta_W = \sqrt{\frac{\pi \alpha}{\sqrt{2} G_F}} \equiv A = 37.28038(1) \text{ GeV}. \quad (33)$$

Since A is practically known exactly (to lowest order) we find the following relations between experimental uncertainties,

$$\frac{\delta M_Z}{M_Z} = \left(2 - \frac{M_Z^2}{M_W^2}\right) \frac{\delta M_W}{M_W} = \frac{\tan^2 \theta_W - 1}{2} \frac{\delta \sin^2 \theta_W}{\sin^2 \theta_W}, \quad \frac{\delta M_W}{M_W} = -\frac{1}{2} \frac{\delta \sin^2 \theta_W}{\sin^2 \theta_W}, \quad (34)$$

so that the M_W error of 15 MeV corresponds rather to measurements of M_Z to 12 MeV precision or to $\sin^2 \theta_{\text{eff}}^\ell$ with an uncertainty of 9×10^{-5} . We conclude that M_W is now the most accurately measured derived quantity in this sector of the EW theory. Of course, relations such as in Eqs. (33) receive important radiative corrections (see the next subsection), making M_W and $\sin^2 \theta_{\text{eff}}^\ell$ fundamentally distinct observables already in the SM (and even more so in the presence of new physics). This is illustrated in Figure 3 where the direct measurements of M_W and m_t are compared with all other EW precision data (dominated by $\sin^2 \theta_{\text{eff}}^\ell$).

Most of the LEP 2 measurements and all of those from the Tevatron use direct kinematical reconstruction. But the LEP Collaborations also performed a W^+W^- threshold scan of the type envisioned with much larger statistics at an International Linear Collider (ILC), where a 5 MeV uncertainty [34] may be reached within only one year. Kinematical fitting at the ILC could contribute an independent determination, likewise with 5 MeV precision, but this would need several years of data taking [35].

The Tevatron combination [33] is strongly dominated by the latest CDF result from Run II [36], $M_W = 80.387 \pm 0.012_{\text{stat.}} \pm 0.010_{\text{syst.}} \pm 0.011_{\text{theo.}}$ GeV, even though this is based on only 2.2 fb^{-1} of integrated luminosity. From past experience one anticipates that the systematic error should scale roughly with statistics [37]. With the full data set based on 10 fb^{-1} one can therefore reasonably expect the total CDF error of 19 MeV to shrink to at least 13 MeV, or even further if there is also progress regarding production theory, namely parton distribution functions (PDFs) and QED radiation. Indeed,

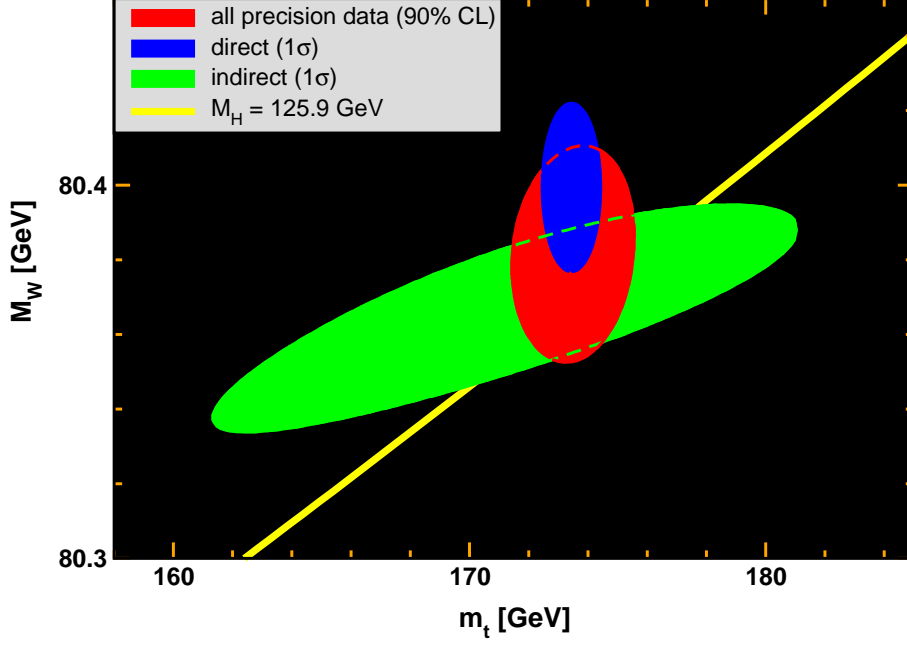


Figure 3: 1σ (39.35% CL) region in M_W as a function of m_t for the direct and indirect determinations, and the 90% CL region ($\Delta\chi^2 = 4.605$) allowed by both data sets. The SM prediction is indicated as the narrow, bright (yellow) band.

while the method was traditionally limited by the lepton energy scale determination, the CDF error is now dominated by the PDF uncertainty. Given these developments, there are also excellent prospects for significant improvements by DØ, as well as for the measurements by ATLAS and CMS at the LHC.

3.3 Implications for the Higgs boson mass

Other SM parameters, such as M_H and m_t , enter into the relations (33) at the level of radiative corrections. Abbreviating, $\hat{s}_Z^2 \equiv \sin^2 \hat{\theta}_W(M_Z)$ and $\hat{c}_Z^2 \equiv \cos^2 \hat{\theta}_W(M_Z)$, one can define radiative correction parameters, Δr [38], $\Delta \hat{r}_W$ and $\Delta \hat{r}$ [39],

$$M_W^2 s_W^2 = M_Z^2 c_W^2 s_W^2 \equiv \frac{A^2}{1 - \Delta r} , \quad M_W^2 \hat{s}_Z^2 \equiv \frac{A^2}{1 - \Delta \hat{r}_W} , \quad M_Z^2 \hat{c}_Z^2 \hat{s}_Z^2 \equiv \frac{A^2}{1 - \Delta \hat{r}} . \quad (35)$$

Note, that all three of these parameters contain a common component $\Delta \hat{\alpha}(M_Z)$, which arises from the renormalization group evolution of α from the Thomson limit to M_Z evaluated in the $\overline{\text{MS}}$ -scheme [40],

$$\hat{\alpha}_Z \equiv \hat{\alpha}(M_Z) = \frac{\alpha}{1 - \Delta \hat{\alpha}(M_Z)} , \quad (36)$$

and introduces a theoretical uncertainty of about $\pm 10^{-4}$ [41] from the hadronic region, as well as the charm and bottom quark thresholds. This induces an uncertainty of ∓ 5 GeV in the extracted M_H . The first of Eqs. (35) shows that $M_W = 80.385 \pm 0.015$ GeV can also be interpreted as a measurement of $\Delta r = 0.03505 \mp 0.00090$. Similarly, after $\sin^2 \theta_{\text{eff}}^\ell$ has been translated with the help of Eq. (28) into

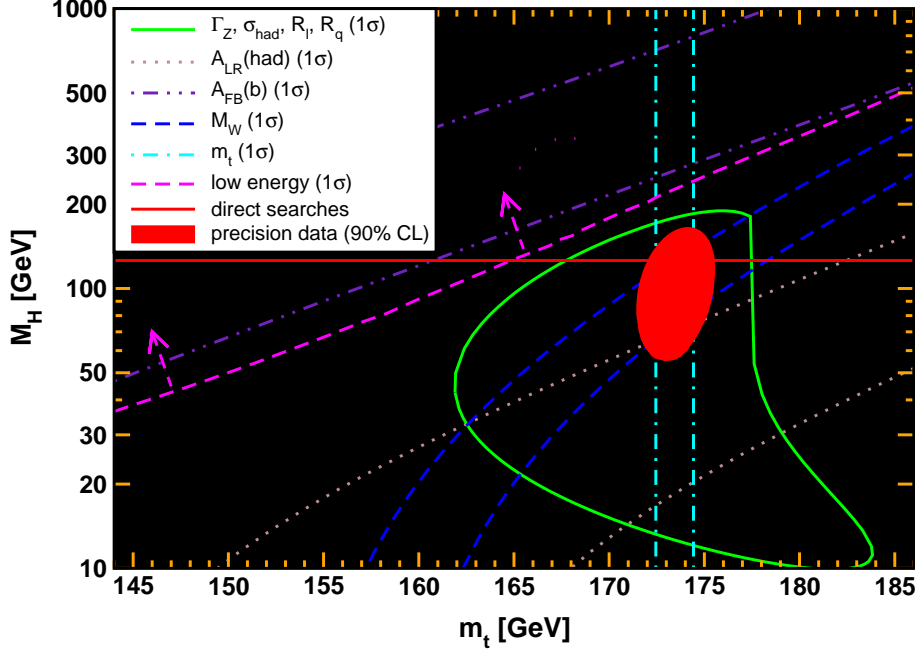


Figure 4: 1σ (39.35% CL) contours of M_H as a function of the top quark pole mass for various inputs, and the 90% CL region ($\Delta\chi^2 = 4.605$) allowed by all data. The horizontal red line reflects the Higgs masses indicated by the LHC events [47,48].

$\hat{s}_Z^2 = 0.23126 \pm 0.00016$, the last of Eqs. (35) implies $\Delta\hat{r} = 0.05982 \pm 0.00045$. Finally, combining the results for M_W and $\sin^2\theta_{\text{eff}}^\ell$ gives $\Delta\hat{r}_W = 0.06994 \pm 0.00073$, but this is not independent of Δr and $\Delta\hat{r}$.

Both, Δr and $\Delta\hat{r}$, are functions of M_H (the leading behavior will be illustrated in Section 3.4) and can therefore be used to constrain it, but both depend quadratically on m_t . Denoting,

$$\rho_t \equiv \frac{N_C}{16\pi^2} \frac{m_t^2}{v^2} = 0.0094 \left(\frac{m_t}{173.21 \text{ GeV}} \right)^2, \quad (37)$$

where $N_C = 3$ is the color factor, one finds for the leading terms, $\Delta r \simeq \Delta\hat{a}(M_Z) - \cot^2\theta_W \rho_t$ and $\Delta\hat{r} \simeq \Delta\hat{a}(M_Z) - \rho_t$, so that m_t needs to be known to very high precision. The various measurements from the Tevatron [42] and the LHC [43] (strongly dominated by the CMS μ +jets channel) combine to,

$$m_t^{\text{Tevatron}} = 173.18 \pm 0.56_{\text{stat}} \pm 0.75_{\text{syst}} \text{ GeV}, \quad m_t^{\text{LHC}} = 173.34 \pm 0.47_{\text{stat}} \pm 1.33_{\text{syst}} \text{ GeV}. \quad (38)$$

Conservatively assuming that the Tevatron systematic error is common to both colliders, one can form a global average,

$$m_t = 173.21 \pm 0.51_{\text{uncorr}} \pm 0.75_{\text{corr}} \pm 0.5_{\text{theo}} \text{ GeV} = 173.2 \pm 1.0 \text{ GeV}, \quad (39)$$

where we have added a theory uncertainty from the relation [44] between the top quark pole mass and the $\overline{\text{MS}}$ -mass (the size of the three-loop term). The latter is used in the EW library, GAPP [45], to minimize theoretical uncertainties. Such a short distance mass definition (unlike the pole mass) is free from non-perturbative and renormalon [46] uncertainties. We are assuming that the kinematic mass

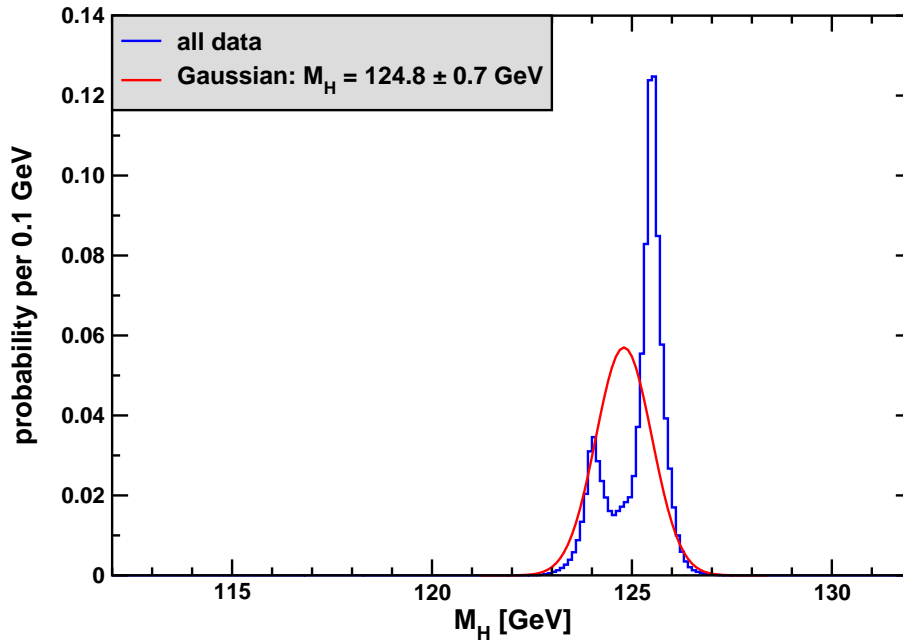


Figure 5: The normalized probability distribution (in blue) of M_H based on all (direct and indirect) data. It is highly non-Gaussian, but one can construct a reference bell curve (shown in red) providing a 1σ estimate of M_H , as well as a measure of significance.

extracted from the collider events corresponds within this uncertainty to the pole mass. Constraints on M_H as a function of m_t are shown in Figure 4 for various data sets.

A global fit to all EW precision data including the observables in Tables 1 and 2, as well as further measurements from high and low energies, gives

$$M_H = 101^{+25}_{-20} \text{ GeV}. \quad (40)$$

The quality of the fit is excellent with a χ^2 of 43.658 for 42 effective degrees of freedom, which translates into a probability for a higher χ^2 of 41%. Reflecting the discussion of the previous paragraph, there is a large (42%) correlation between M_H and m_t . The fit value (40) is slightly lower (by 1.0σ) than the

$$M_H = 124.8 \pm 0.7 \text{ GeV}, \quad (41)$$

suggested [49] by the Higgs boson candidates seen at the LHC [47,48]. Indeed, if one combines the precision data with the direct Higgs boson search results from LEP 2 [50], the Tevatron [51], and the LHC [47,48], one can construct the proper probability density [49] shown in Figure 5. The distribution shows two peaks (traceable to the two LHC experiments) and is highly non-Gaussian not only in the bulk but also (and more importantly) in the tails where further local maxima occur. By cutting the distribution off where it falls below the density of the highest such local maximum defines a signal region. The integral under this signal region and its center define a reference Gaussian, which is also shown in the Figure. Moreover, one can now unambiguously find the number of standard deviations corresponding to the signal region, giving rise to a significance of 3.4σ . This method [49] avoids the poorly defined look-elsewhere effect correction which needs to be applied by the LHC Collaborations.

3.4 Implications for physics beyond the Standard Model

The parameters, Δr , $\Delta \hat{r}_W$ and $\Delta \hat{r}$, introduced in the previous subsection, are also possibly affected by and can provide constraints on hypothetical particles beyond the SM which may appear in loop corrections to the transverse parts of the current-current correlators (*i.e.*, in the so-called oblique corrections),

$$\hat{\Pi}_{\gamma\gamma}^{\text{new}}(q^2) \equiv \frac{g^2}{2} \langle J^A J^A \rangle, \quad \hat{\Pi}_{\gamma Z}^{\text{new}}(q^2) \equiv \frac{g^2}{2} \langle J^A J^Z \rangle, \quad (42)$$

$$\hat{\Pi}_{ZZ}^{\text{new}}(q^2) \equiv \frac{g^2}{2} \langle J^Z J^Z \rangle, \quad \hat{\Pi}_{WW}^{\text{new}}(q^2) \equiv \frac{g^2}{2} \langle J^W J^W \rangle. \quad (43)$$

Consider first the WW and ZZ self-energies. Since at present precise measurements are available only at low (basically vanishing) energies and at the EW scale, one is left with $\hat{\Pi}_{WW}^{\text{new}}(0)$, $\hat{\Pi}_{WW}^{\text{new}}(M_W^2)$, $\hat{\Pi}_{ZZ}^{\text{new}}(0)$ and $\hat{\Pi}_{ZZ}^{\text{new}}(M_Z^2)$. These are infinite (their UV-divergencies can be absorbed in the counterterm related to G_F) but appropriately chosen differences are finite,

$$\Delta \hat{r}_W^{\text{new}} = \frac{\hat{\Pi}_{WW}^{\text{new}}(M_W^2) - \hat{\Pi}_{WW}^{\text{new}}(0)}{M_W^2} \equiv \frac{\alpha}{4\hat{s}_Z^2} S_W, \quad \Delta \hat{r}_Z^{\text{new}} \equiv \frac{\hat{\Pi}_{ZZ}^{\text{new}}(M_Z^2) - \hat{\Pi}_{ZZ}^{\text{new}}(0)}{M_Z^2} \equiv \frac{\alpha}{4\hat{s}_Z^2 \hat{c}_Z^2} S_Z, \quad (44)$$

$$\Delta \hat{\rho}^{\text{new}} = \frac{\hat{\Pi}_{WW}^{\text{new}}(M_W^2) - \hat{c}_Z^2 \hat{\Pi}_{ZZ}^{\text{new}}(M_Z^2)}{M_W^2}, \quad \Delta \rho^{\text{new}} = \frac{\hat{\Pi}_{WW}^{\text{new}}(0) - \hat{c}_Z^2 \hat{\Pi}_{ZZ}^{\text{new}}(0)}{M_W^2(1 - \Delta \hat{r}_W)} \equiv \frac{\alpha T}{1 - \Delta \hat{r}_W} \approx \hat{\alpha}_Z T, \quad (45)$$

$$\Delta \hat{r}^{\text{new}} = \hat{\rho}(\Delta \hat{r}_W^{\text{new}} - \Delta \hat{\rho}^{\text{new}}) = \frac{1}{M_Z^2} \left[\hat{\Pi}_{ZZ}^{\text{new}}(M_Z^2) - \frac{\hat{\Pi}_{WW}^{\text{new}}(0)}{\hat{c}_Z^2} \right] = \alpha \left(\frac{S_Z}{4\hat{s}_Z^2 \hat{c}_Z^2} - \hat{\rho} T \right), \quad (46)$$

so that only three are independent [52–55]. For these formulae, we defined the classic ρ parameter [56] describing the ratio of neutral-to-charged current interaction strengths in analogy to the high-energy $\hat{\rho}$ parameter [39],

$$\hat{\rho} \equiv \frac{1}{1 - \Delta \hat{\rho}} \equiv \frac{\hat{c}_W^2}{\hat{c}_Z^2} = \frac{1 - \Delta \hat{r}}{1 - \Delta \hat{r}_W}, \quad \rho \equiv \frac{1}{1 - \Delta \rho} \equiv \frac{G_{\text{NC}}}{G_F} \equiv \frac{1 - \Delta \hat{r}}{1 - \Delta \hat{r}_Z}, \quad (47)$$

and kept track of reducible higher-order effects, so that

$$M_Z^2 \hat{c}_Z^2 \hat{s}_Z^2 = \frac{A^2}{1 - \Delta \hat{r}} = \frac{A^2}{\hat{\rho}(1 - \Delta \hat{r}_W)} = \frac{A^2}{\rho(1 - \Delta \hat{r}_Z)} \quad (48)$$

exactly. It is understood that these new physics contributions are to be added to the SM ones (*i.e.*, not to be written in factorized form) and that therefore the self-energies are normalized with α rather than $\hat{\alpha}_Z$. The dominant SM contributions to the oblique parameters for the cases of a heavy top quark and a heavy Higgs boson are given by,

$$\Delta \hat{r}_W \approx \Delta \hat{\alpha}(M_Z) + \frac{\alpha}{48\pi \hat{s}_Z^2} \ln \frac{M_H^2}{M_Z^2}, \quad \Delta \hat{r}_Z \approx \Delta \hat{\alpha}(M_Z) + \frac{\alpha}{48\pi \hat{s}_Z^2 \hat{c}_Z^2} \ln \frac{M_H^2}{M_Z^2}, \quad (49)$$

$$\Delta r \approx \Delta \hat{\alpha}(M_Z) + \frac{11\alpha}{48\pi \hat{s}_Z^2} \ln \frac{M_H^2}{M_Z^2} - \frac{\hat{c}_Z^2}{\hat{s}_Z^2} \rho_t, \quad \Delta \rho \approx \rho_t - \frac{3\hat{\alpha}_Z}{16\pi \hat{c}_Z^2} \ln \frac{M_H^2}{M_Z^2}. \quad (50)$$

A non-vanishing T is associated with new physics disrespecting the custodial symmetry mentioned in Section 2.2, such as from mass splittings within iso-doublets or higher-dimensional Higgs representations. Experimentally, T can be separated from S_Z in Eq. (46) by low-energy neutral current processes. One can also use the Z -width, Γ_Z , which through Z -boson wave-function renormalization is affected by the

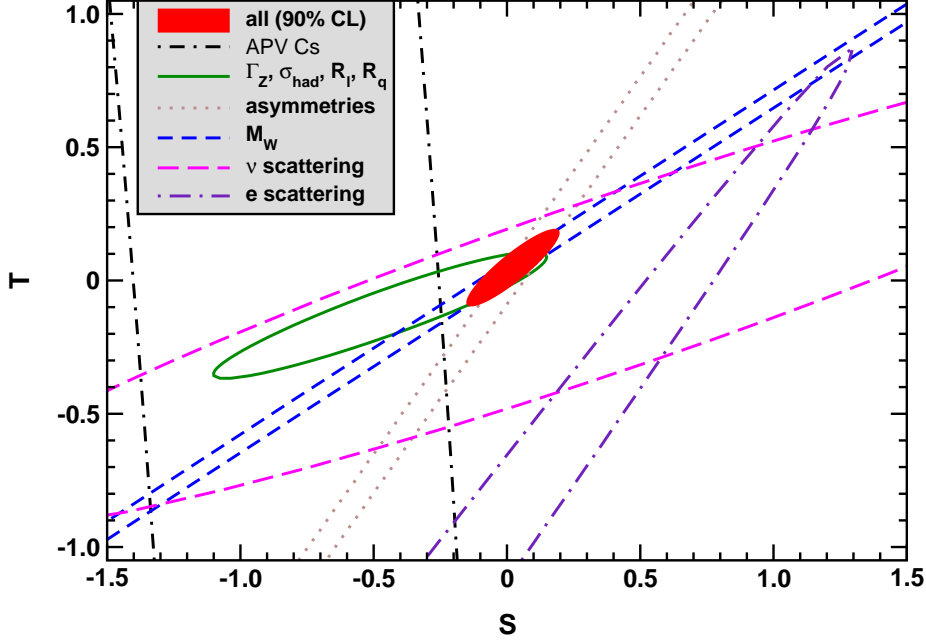


Figure 6: 1σ regions in S and T from various inputs. Data sets not involving M_W or Γ_W are insensitive to U . The strong coupling constant, $\hat{\alpha}_s(M_Z)$, is constrained by using the τ lifetime as additional input. This allows Γ_Z , the hadronic Z -peak cross-section, σ_{had} , and the R_q , to provide additional new physics probes rather than fixing $\hat{\alpha}_s$. The long-dash-dotted (indigo) contour from polarized e scattering [59,60] is the upper tip of an elongated ellipse centered at $S \approx -14$ and $T \approx -20$. It may look as if it is deviating strongly but it is off by only 1.8σ , an illusion arising because $\Delta\chi^2 > 0.77$ throughout the visible part of the contour.

derivative of $\hat{\Pi}_{ZZ}^{\text{new}}(q^2)$. To the extent to which this differs from the difference defining S_Z in Eq. (44), there would then be an additional measurable parameter, called V [57]. A similar remark applies to $\hat{\Pi}_{WW}^{\text{new}}(q^2)$ where the difference in Eq. (44) and its derivative give rise to the parameters S_W [52] and W [57], respectively. However, new physics at a very high scale, Λ_{new} , will affect S_Z and V (or S_W and W) in very similar ways, and only S_W , S_Z and T survive when one additionally assumes the oblique new physics to be very heavy.

This case also greatly simplifies the analysis for the QED vacuum polarization tensor,

$$\hat{\Pi}_{\gamma\gamma}^{\text{new}}(q^2) = \hat{\Pi}_{\gamma\gamma}^{\text{new}}(0) + q^2 \frac{d}{dq^2} \hat{\Pi}_{\gamma\gamma}^{\text{new}}(q^2) \Big|_{q^2=0} + \mathcal{O}\left(\frac{q^4}{\Lambda_{\text{new}}^4}\right), \quad (51)$$

where the first term vanishes as a consequence of the QED Ward identity, while the remaining term can be absorbed into the $\overline{\text{MS}}$ -definition, $\hat{\alpha}_Z$, of the gauge coupling. Parallel remarks apply to $\hat{\Pi}_{\gamma Z}^{\text{new}}(q^2)$ whose effects are absorbed into \hat{s}_Z^2 , but as was the case before with the V and W parameters, relatively light new physics may, at least in principle, separate differences from derivatives (or equivalently allow higher orders in $\Lambda_{\text{new}}^{-1}$) giving rise to what is called the X parameter [57].

Finally, similar observations can be made about the vector parts of $\hat{\Pi}_{ZZ}^{\text{new}}(q^2)$ and $\hat{\Pi}_{WW}^{\text{new}}(q^2)$, so that in the limit $\Lambda_{\text{new}} \rightarrow \infty$ the parameters S_W and S_Z are only affected by new physics breaking axial

Table 3: Result of a global fit to the three parameters for heavy oblique new physics and their correlations. The agreement with the SM prediction, $S = T = U = 0$, is remarkable.

parameter	global fit result	correlation matrix		
S	0.00 ± 0.10	1.00	0.91	-0.55
T	0.02 ± 0.11	0.91	1.00	-0.79
U	0.04 ± 0.09	-0.55	-0.79	1.00

$SU(2)_L$ [53]. The combination [55] given by $U \equiv S_W - S_Z = \Delta\hat{\rho} - \Delta\rho$ manifestly breaks the vector part, as well, and in this sense U can be regarded as second order in the new physics and is expected to be small. This is borne out in concrete scenarios of dominantly oblique new physics like technicolor, extra fermion generations, or additional Higgs multiplets, with U often of similar size as the usually neglected parameters V , W , and X [57]. Thus, one frequently reduces the analysis allowing only $S \equiv S_Z$ and T , as illustrated in Figure 6. The current three parameter fit result is shown in Table 3. Note, that contributions to S are not decoupling. *E.g.*, a degenerate extra fermion generation contributes $S = 2/3\pi$ independently of the fermion masses and is excluded along with many technicolor models.

In the above discussion, we have implicitly assumed that the new physics is at or above the EW scale. Another possibility is that there are new particles with masses much lighter than M_Z , as long as they are very weakly coupled. An example of this [58] would be a “dark- Z ” boson with no direct SM fermion couplings, but both kinetic and mass mixing effects with the photon and the ordinary Z . It could affect the predicted value of the weak mixing angle at low energies in terms of \hat{s}_Z^2 and would therefore contribute to the X parameter.

4 Neutrino scattering

The gauge and Higgs boson properties reviewed in Section 3 strongly constrain new physics scenarios that may alter them. This may occur through mixing or by otherwise modifying the tree-level relations of the SM. The quantum oblique corrections discussed in Section 3.4 are another possibility.

On the other hand, there may be new particles beyond the SM which mostly generate new amplitudes without strongly affecting the masses and couplings of the W and Z bosons. Then the new physics would not be resonating and one best studies processes away from the Z -pole. This may be at the hadron colliders, Tevatron and LHC, *i.e.*, at the current energy frontier, but lower energy processes typically have the advantage of much higher rates. To screen the EW and possibly the new physics from the electromagnetic and strong interactions one either probes with neutrinos or utilizes violations of symmetries such as parity and CP. This will be discussed, respectively, in the present and in the following section (previous reviews can be found in Refs. [2,15,30]).

High-energy neutrino beams are produced by directing protons of very high energy on a fixed target from which pions and kaons emerge as secondary beams. These tend to be positively charged so that it is easier to make high-intensity ν_μ than $\bar{\nu}_\mu$ beams (one needs to correct for small ν_e and $\bar{\nu}_e$ contaminations). If the decaying mesons are energy selected the neutrino energies can be constrained (narrow band beams) to some extent, but one still needs to measure the final state μ^\pm momenta to reliably determine E_ν . This is not an option, however, for the deep-inelastic scattering (DIS) of neutrinos from hadrons or nuclei mediated by the neutral current so that here one focuses on integrated cross-sections and their ratios. A future direction are neutrino factories [61] where muons decay in primary beams, allowing better knowledge of the ν -spectra and a composition of exactly 50% ν_μ and $\bar{\nu}_e$.

4.1 Neutrino-electron scattering

The elastic scattering of ν_μ or $\bar{\nu}_\mu$ from electrons [62] is at the leading order mediated by the weak neutral current (NC), which in turn was discovered through a single $\bar{\nu}_\mu$ event of this kind at CERN [63]. From the second Eq. (25) one can glean the relevant interaction⁶ (in the limit of vanishing ν masses),

$$\begin{aligned} \mathcal{L}_{\text{NC}}^{\nu_\mu e} = & -2 \frac{\cos^2 \theta_W}{v^2} \bar{\nu}_\mu \gamma^\rho \frac{g_V^{\nu_\mu} - g_A^{\nu_\mu} \gamma^5}{2} \nu_\mu \bar{e} \gamma_\rho \frac{g_V^e - g_A^e \gamma^5}{2} e = \\ & - \frac{2}{v^2} \bar{\nu}_\mu \gamma^\rho P_L \nu_\mu \bar{e} \gamma_\rho \frac{g_{LV}^{\nu_\mu e} - g_{LA}^{\nu_\mu e} \gamma^5}{2} e = - \frac{2}{v^2} \bar{\nu}_{\mu L} \gamma^\rho \nu_{\mu L} [g_{LL}^{\nu_\mu e} \bar{e}_L \gamma_\rho e_L + g_{LR}^{\nu_\mu e} \bar{e}_R \gamma_\rho e_R], \end{aligned} \quad (52)$$

where the SM tree-level relations for the coefficients of these effective four-Fermi operators are given by,

$$g_{LL}^{\nu_\mu e} \equiv \cos^2 \theta_W g_L^{\nu_\mu} g_L^e = -\frac{1}{2} + \sin^2 \theta_W, \quad g_{LR}^{\nu_\mu e} \equiv \cos^2 \theta_W g_L^{\nu_\mu} g_R^e = \sin^2 \theta_W, \quad (53)$$

$$g_{LV}^{\nu_\mu e} \equiv g_{LL}^{\nu_\mu e} + g_{LR}^{\nu_\mu e} = -\frac{1}{2} + 2 \sin^2 \theta_W, \quad g_{LA}^{\nu_\mu e} \equiv g_{LL}^{\nu_\mu e} - g_{LR}^{\nu_\mu e} = -\frac{1}{2}. \quad (54)$$

The first index L is redundant in the absence of right-handed neutrinos (or when their masses are very large) and therefore it is often dropped. Experimentally, one can separate these couplings by using spectral information or by comparing the ν_μ and $\bar{\nu}_\mu$ rates. For example, in the ultra-relativistic regime, $E_\nu \gg m_e$, and for events which scatter strictly in the forward direction, helicity conservation implies that only left-handed (right-handed) electrons can participate in ν ($\bar{\nu}$)-scattering, thus filtering out $g_{LL}^{\nu_\mu e}$ ($g_{LR}^{\nu_\mu e}$). In general, the differential neutrino scattering cross-section in the laboratory frame reads [64],

$$\frac{d\sigma(\nu e^- \rightarrow \nu e^-)}{dy} = \frac{m_e E_\nu}{\pi v^4} \left[(g_{LL}^{\nu_\mu e})^2 + (g_{LR}^{\nu_\mu e})^2 (1-y)^2 - g_{LL}^{\nu_\mu e} g_{LR}^{\nu_\mu e} \frac{m_e}{E_\nu} y \right], \quad (55)$$

where we neglected $-q^2$ against M_W in the W -propagator, and where the Lorentz-invariant quantity,

$$y \equiv \frac{p_e(p_\nu - p'_\nu)}{p_e p_\nu} \equiv \frac{p_e q}{p_e p_\nu} = \frac{-q^2}{2p_e p_\nu} = 1 - \frac{E'_\nu}{E_\nu} = \frac{E'_e - m_e}{E_\nu}, \quad 0 \leq y \leq \left(1 + \frac{m_e}{2E_\nu}\right)^{-1}, \quad (56)$$

is the relative neutrino energy transfer in terms of the initial neutrino and electron 4-momenta, p_ν and p_e , and their primed final state counterparts. The $\bar{\nu}$ cross-section has exactly the same form as Eq. (55) except for the interchange $g_{LL}^{\nu_\mu e} \leftrightarrow g_{LR}^{\nu_\mu e}$. In the ultra-relativistic limit, this integrates to

$$\sigma(\nu e^- \rightarrow \nu e^-) = \frac{m_e E_\nu}{\pi v^4} \left[(g_{LL}^{\nu_\mu e})^2 + \frac{(g_{LR}^{\nu_\mu e})^2}{3} \right], \quad \sigma(\bar{\nu} e^- \rightarrow \bar{\nu} e^-) = \frac{m_e E_{\bar{\nu}}}{\pi v^4} \left[\frac{(g_{LL}^{\nu_\mu e})^2}{3} + (g_{LR}^{\nu_\mu e})^2 \right], \quad (57)$$

Thus, the small m_e strongly suppresses the cross-sections which do not exceed half a fb even for 300 GeV incident neutrinos, and event rates of only a few thousand have been achieved. With future neutrino beams of about a factor of 100 higher intensity, so-called *superbeams*, the errors would decrease by an order of magnitude and very competitive results would become possible. Yet higher precision could be obtained at a neutrino factory [61].

The most precise measurements (shown in Table 4) are from the CHARM [65] and CHARM II [66] Collaborations at CERN and the BNL-734 (CALO) experiment [67]. In addition to these NC results, the CC *inverse muon-decay* cross-section, $\sigma(\nu_\mu e^- \rightarrow \nu_e \mu^-)$, is needed in conjunction with ordinary muon-decay to establish the $V - A$ structure of the weak charged current unambiguously. It is given by Eq. (57) with the square bracket dropped.

⁶In order to suppress some spurious factors of $\sqrt{2}$ we normalize the low-energy Lagrangians in terms of v rather than G_F , with the understanding that a renormalization scheme is used so that Eq. (13) holds to all orders.

Table 4: Results of the most precise $\nu_\mu e$ and $\bar{\nu}_\mu e$ scattering experiments and their combinations. The SM predictions are given by $g_{LV}^{\nu_\mu e} = -0.0396$ and $g_{LA}^{\nu_\mu e} = -0.5064$.

Group	Ref.	Laboratory	Accelerator	$g_{LV}^{\nu_\mu e}$	$g_{LA}^{\nu_\mu e}$
CHARM	[65]	CERN	SpS	$-0.06 \pm 0.07 \pm 0.02$	$-0.54 \pm 0.04 \pm 0.06$
CHARM II	[66]	CERN	SpS	-0.035 ± 0.017	-0.503 ± 0.017
CALO	[67]	BNL	AGS	$-0.107 \pm 0.035 \pm 0.028$	$-0.514 \pm 0.023 \pm 0.028$
all		both	both	-0.045 ± 0.016	-0.507 ± 0.015

For $\nu_e e$ and $\bar{\nu}_e e$ elastic scattering there is an extra contribution from the weak charged current (CC),

$$\mathcal{L}_{\text{NC+CC}}^{\nu_e e} = -2 \frac{\cos^2 \theta_W}{v^2} \bar{\nu}_e \gamma^\rho \frac{g_V^{\nu_e} - g_A^{\nu_e} \gamma^5}{2} \nu_e \bar{e} \gamma_\rho \frac{g_V^e - g_A^e \gamma^5}{2} e - \frac{2}{v^2} \bar{\nu}_e \gamma^\rho P_L e \bar{e} \gamma_\rho P_L \nu_e, \quad (58)$$

which in the SM appears naturally in charge-changing order, but can be brought into the charge-retention form of Eq. (52) by means of a Fierz re-ordering (in fact, the second term in Eq. (58) is Fierz invariant), and one finds at the SM tree-level,

$$g_{LV}^{\nu_e e} \equiv \cos^2 \theta_W g_L^{\nu_e} g_V^e + 1 = \frac{1}{2} + 2 \sin^2 \theta_W, \quad g_{LA}^{\nu_e e} \equiv \cos^2 \theta_W g_L^{\nu_e} g_A^e + 1 = \frac{1}{2}. \quad (59)$$

The $\nu_e e$ process has been measured by the CNTR (LAMPF) [68] and LSND (LANSCE) [69] experiments at LANL, while $\bar{\nu}_e e$ scattering was studied by the TEXONO Collaboration [70] at the Kuo-Sheng Nuclear Power Reactor in Taiwan. These experiments are generally less precise than those using ν_μ or $\bar{\nu}_\mu$ -beams, but as shown in Figure 7, they are very useful to reduce the four-fold ambiguity from $g_{V,A} \rightarrow -g_{V,A}$ and $g_{V,A} \rightarrow g_{A,V}$ to only two solutions. The interference term between the neutral and charged current amplitudes could also be extracted [69].

The tree-level relations (53), (54) and (59) are subject to the EW radiative corrections discussed in Section 4.3. The remaining QED corrections have been obtained in the ultra-relativistic limit in Ref. [64] (which also gives corrections to the spectrum), and are assumed to be removed beforehand.

4.2 Deep-inelastic neutrino-nucleus scattering and related processes

The most direct way to access the ν -quark sector is in the deep-inelastic kinematic regime [71,72], where neutrinos scatter in a first approximation incoherently from individual quarks. The use of heavy nuclei such as iron increases interaction rates compared to the leptonic processes covered in the previous section where lower density materials such as glass are preferred to facilitate better angular resolution of the showers produced by the recoil electrons. Even more importantly, the cross-sections will be seen to be proportional to the nucleon mass rather than m_e .

On the other hand, while CC events can be reconstructed from the recoiling muons and the hadronic energy, NC events cannot. Moreover, there are many complications due to hadronic and nuclear structure effects, and one resorts to cross-section ratios involving both neutral and charged currents in which many of the associated uncertainties cancel. Suppressing family indices, the relevant quark-level effective Lagrangians are given by,

$$\mathcal{L}_{\text{CC}}^{\nu q} = -\frac{2}{v^2} \left[\bar{e} \gamma^\mu \frac{1 - \gamma^5}{2} \nu \bar{u} \gamma_\mu \frac{1 - \gamma^5}{2} V_{\text{CKM}} d + \text{H.c.} \right], \quad (60)$$

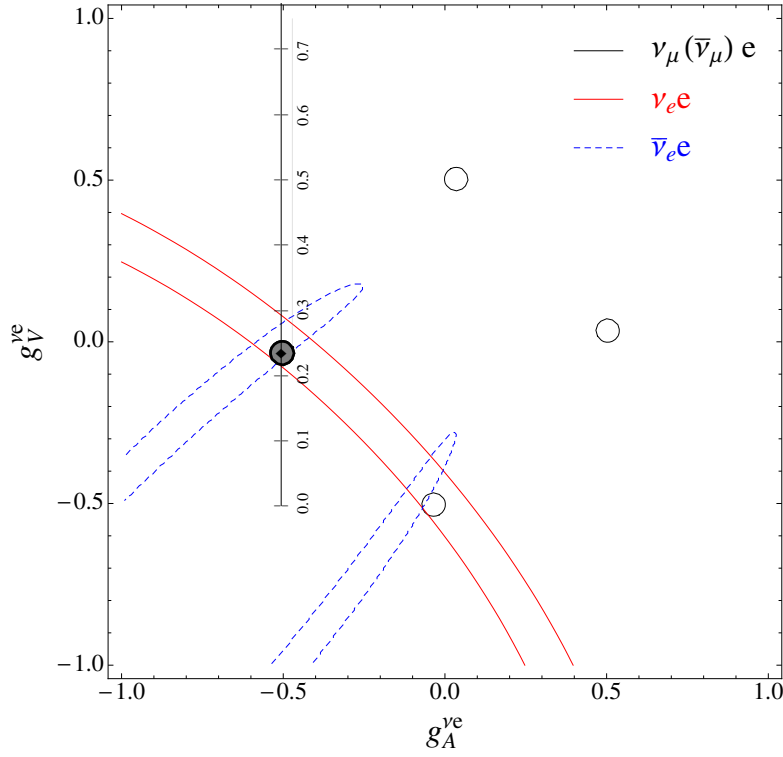


Figure 7: Allowed contours in $g_V^{\nu e}$ vs. $g_A^{\nu e}$ from neutrino-electron scattering and the SM prediction as a function of the weak mixing angle \hat{s}_Z^2 (the SM best fit value $\hat{s}_Z^2 = 0.23116$ is also indicated). The $\nu_e e$ [68,69] and $\bar{\nu}_e e$ [70] constraints are at 1σ while each of the four equivalent $\nu_\mu(\bar{\nu}_\mu)e$ solutions ($g_{V,A} \rightarrow -g_{V,A}$ and $g_{V,A} \rightarrow g_{A,V}$) are at 90% CL. The global best fit region (shaded) almost exactly coincides with the corresponding $\nu_\mu(\bar{\nu}_\mu)e$ region. The solution near $g_A = 0$, $g_V = -0.5$ is eliminated by $e^+e^- \rightarrow \ell^+\ell^-$ data under the weak additional assumption that the neutral current is dominated by the exchange of a single Z boson. (Figure reprinted as permitted according to journal guidelines from *Phys. Rev. D* 86 (2012) 010001, J. Erler and P. Langacker [15].)

$$\begin{aligned} \mathcal{L}_{\text{NC}}^{\nu q} = & -\frac{2}{v^2} \bar{\nu} \gamma^\mu \frac{1-\gamma_5}{2} \nu \left[\bar{u} \gamma_\mu \frac{g_{LV}^{\nu u} - g_{LA}^{\nu u} \gamma_5}{2} u + \bar{d} \gamma_\mu \frac{g_{LV}^{\nu d} - g_{LA}^{\nu d} \gamma_5}{2} d \right] = \\ & -\frac{2}{v^2} \bar{\nu} \gamma^\mu \nu_L \left[g_{LL}^{\nu u} \bar{u}_L \gamma_\mu u_L + g_{LR}^{\nu u} \bar{u}_R \gamma_\mu u_R + g_{LL}^{\nu d} \bar{d}_L \gamma_\mu d_L + g_{LR}^{\nu d} \bar{d}_R \gamma_\mu d_R \right], \end{aligned} \quad (61)$$

where the SM relations for the real-valued coefficients in Eq. (61) are,

$$g_{LL}^{\nu u} \equiv \frac{g_{LV}^{\nu u} + g_{LA}^{\nu u}}{2} = \frac{1}{2} - \frac{2}{3} \sin^2 \theta_W, \quad g_{LR}^{\nu u} \equiv \frac{g_{LV}^{\nu u} - g_{LA}^{\nu u}}{2} = -\frac{2}{3} \sin^2 \theta_W, \quad (62)$$

$$g_{LL}^{\nu d} \equiv \frac{g_{LV}^{\nu d} + g_{LA}^{\nu d}}{2} = -\frac{1}{2} + \frac{1}{3} \sin^2 \theta_W, \quad g_{LR}^{\nu d} \equiv \frac{g_{LV}^{\nu d} - g_{LA}^{\nu d}}{2} = \frac{1}{3} \sin^2 \theta_W. \quad (63)$$

One can generalize Eq. (55) to ν -nucleon scattering by introducing proton PDFs, $q(x)$, which are functions of the Bjorken scaling variable (p_N and m_N are the nucleon momenta and mass, respectively),

$$x \equiv \frac{-q^2}{2p_N q} = \frac{-q^2}{2m_N(E_{\text{had}} - m_N)}, \quad 0 \leq x \leq 1. \quad (64)$$

One also defines the *inelasticity* parameter,

$$y \equiv \frac{p_N q}{p_N p_\nu} = \frac{-q^2}{2x p_N p_\nu} = 1 - \frac{E'_\nu}{E_\nu} = \frac{E_{\text{had}} - m_N}{E_\nu}, \quad 0 \leq y \leq \left(1 + \frac{x m_N}{2E_\nu}\right)^{-1}, \quad (65)$$

which is to be compared with the parameter defined in Eq. (56). One then has for νp -scattering,

$$\frac{d^2\sigma(\nu p \rightarrow \nu X)}{dx dy} = \frac{m_p E_\nu}{\pi v^4} \sum_q x \left\{ [(g_{LL}^{\nu q})^2 + (g_{LR}^{\nu q})^2(1-y)^2] q(x) + [(g_{LR}^{\nu q})^2 + (g_{LL}^{\nu q})^2(1-y)^2] \bar{q}(x) \right\}. \quad (66)$$

The $\bar{\nu}p$ cross-section is again implied by interchanging $g_{LL}^{\nu q}$ and $g_{LR}^{\nu q}$, while the neutron case is obtained from these under the assumption of *charge symmetry* by exchanging the u and d quark PDFs, and likewise for the anti-quarks. Top and bottom quarks can safely be neglected, and when one also ignores the second generation quarks, then one can write on average per nucleon, N , in an isoscalar target [73],

$$\begin{aligned} \frac{d^2\sigma(\nu N \rightarrow \nu X)}{dx dy} &= \frac{m_N E_\nu}{2\pi v^4} \left\{ [g_L^2 + g_R^2(1-y)^2] [xu(x) + xd(x)] + [g_R^2 + g_L^2(1-y)^2] [x\bar{u}(x) + x\bar{d}(x)] \right\} \\ &= g_L^2 \frac{d\sigma(\nu N \rightarrow \mu^- X)}{dx dy} + g_R^2 \frac{d\sigma(\bar{\nu} N \rightarrow \mu^+ X)}{dx dy}, \end{aligned} \quad (67)$$

where it was used that (anti)-neutrinos can only emit W^+ (W^-) bosons and thus can only be absorbed by negatively (positively) charged quarks and anti-quarks. In Eq. (67) we abbreviated,

$$g_L^2 \equiv (g_{LL}^{\nu u})^2 + (g_{LL}^{\nu d})^2, \quad g_R^2 \equiv (g_{LR}^{\nu u})^2 + (g_{LR}^{\nu d})^2, \quad (68)$$

$$h_L^2 \equiv (g_{LL}^{\nu u})^2 - (g_{LL}^{\nu d})^2, \quad h_R^2 \equiv (g_{LR}^{\nu u})^2 - (g_{LR}^{\nu d})^2, \quad (69)$$

and with the analogous result for $\bar{\nu}N$ scattering, one arrives at the Llewellyn Smith relations [73],

$$R_\nu \equiv \frac{\sigma(\nu N \rightarrow \nu X)}{\sigma(\nu N \rightarrow \mu^- X)} = g_L^2 + r g_R^2, \quad R_{\bar{\nu}} \equiv \frac{\sigma(\bar{\nu} N \rightarrow \bar{\nu} X)}{\sigma(\bar{\nu} N \rightarrow \mu^+ X)} = \frac{g_R^2}{r} + g_L^2, \quad (70)$$

in terms of the CC cross-section ratio, r , which cancels in the Paschos-Wolfenstein ratios, R_\pm [74],

$$r \equiv \frac{\sigma(\bar{\nu} N \rightarrow \mu^+ X)}{\sigma(\nu N \rightarrow \mu^- X)}, \quad R_\pm \equiv \frac{\sigma(\nu N \rightarrow \nu X) \pm \sigma(\bar{\nu} N \rightarrow \bar{\nu} X)}{\sigma(\nu N \rightarrow \mu^- X) \pm \sigma(\bar{\nu} N \rightarrow \mu^+ X)} = \frac{R_\nu \pm r R_{\bar{\nu}}}{1 \pm r} = g_L^2 \pm g_R^2. \quad (71)$$

In the absence of sea quarks and for an ideal experiment with full acceptance, $r = 1/3$ (*cf.*, Eq. (57)), but r grows almost linearly with the ratio of the fraction of the nucleon's momentum carried by anti-quarks to that carried by quarks, and typically decreases with realistic acceptances. In practice, $r \sim 0.4$ is determined experimentally. The ratio R_- is particularly clean, since any effect shifting $\sigma(\nu N \rightarrow \nu X)$ and $\sigma(\bar{\nu} N \rightarrow \bar{\nu} X)$ equally, drops out.

As for R_ν and $R_{\bar{\nu}}$ individually, the s and c quarks cause effects due to $V_{\text{CKM}} \neq 1$, induce the leading theoretical uncertainty through the non-vanishing charm quark mass, and require knowledge of the strange sea and its asymmetry, $xs(x) - x\bar{s}(x)$. Furthermore, it is necessary to account for the imperfect cancellation of the M_W and M_Z propagator effects, as well as for $m_\mu \neq 0$, $m_N \neq 0$, non-isoscalarity due to the neutron excess in heavy nuclei, and the x and Q^2 dependences of the PDFs. In the approximation of charge symmetry, higher-order QCD corrections are suppressed by $\sin^4 \theta_W$ [75]. Non-perturbative (higher-twist) QCD effects cause, *e.g.*, a violation of the Callan-Gross relation [76] and therefore non-vanishing longitudinal structure functions, but their effects on Eqs. (70) are suppressed for large Q^2 . Most difficult to quantify are charge symmetry violations (from $Q_d \neq Q_u$ [77] and from $m_d \neq m_u$ [78]) and nuclear effects (including medium modification of the nucleon PDFs [79]). EW and QED radiative

Table 5: Results of the most precise isoscalar ν DIS experiments as quoted in the original publications and the SM predictions adjusted to the applicable Q^2 values as explained in Section 4.3. The CCFR experiment was mostly sensitive to R_ν and quotes the combination $\kappa = 1.7897 g_L^2 + 1.1479 g_R^2 - 0.0916 h_L^2 - 0.0782 h_R^2$. In all cases, additional theory corrections and uncertainties may have to be applied as discussed in the text.

Group	Ref.	Laboratory	Accelerator	Target	Quantity	Measurement	SM
CHARM	[82]	CERN	SpS	CaCO ₃	R_ν	0.3093 ± 0.0031	0.3156
CDHS	[83]	CERN	SpS	Fe	R_ν	0.3072 ± 0.0033	0.3091
CCFR	[84]	FNAL	Tevatron	BeO	κ	0.5820 ± 0.0041	0.5830
NuTeV	[85]	FNAL	Tevatron	BeO	g_L^2	0.30005 ± 0.00137	0.3039
NuTeV	[85]	FNAL	Tevatron	BeO	g_R^2	0.03076 ± 0.00110	0.0300

corrections [80,81], beyond those treated in Section 4.3, are large and kinematics dependent, and have to be applied by the experimentalists.

The results of the most precise ν DIS experiments on isoscalar targets are summarized in Table 5. Note, that there is a 2.7σ deviation in the NuTeV determination of g_L^2 . This corresponds to the result of the original NuTeV publication [85]. Corrections of the kind discussed in the previous paragraph that go beyond those already considered in the original analysis have not been applied in Table 5.

Determinations of the isovector combinations are more difficult since the experiments are harder to interpret theoretically. They can be constrained by using ν DIS from non-isoscalar targets (see *e.g.*, Ref. [86]), but there is more model dependence.

Another possibility is in principle the elastic scattering of neutrinos from protons [87]. At very low Q^2 these experiments are sensitive to the combination, $(g_{LV}^{\nu p})^2 + g_A^2 (g_{LA}^{\nu p})^2 (1 + \Delta S_s)^2$, where

$$g_{LV}^{\nu p} \equiv 2g_{LV}^{\nu u} + g_{LV}^{\nu d} = \frac{1}{2} - 2 \sin^2 \theta_W, \quad g_{LA}^{\nu p} \equiv 2g_{LA}^{\nu u} + g_{LA}^{\nu d} = \frac{1}{2}, \quad (72)$$

and where $g_A = 1.27$ is the axial-vector coupling constant as measured in neutron decays (the right hand sides show the SM tree-level). ΔS_s is the strange quark contribution to the nucleon spin which is poorly known. One can try to separate $(g_{LV}^{\nu p})^2$ from the axial contributions kinematically by exploiting the different behavior at $Q^2 \neq 0$. Unfortunately, this induces further parameters, such as the nucleon axial dipole mass, M_A , and the strange quark electric and magnetic form factors, even though lattice calculations [88,89] indicate that the latter are rather small⁷. At this level, one also faces the neutron combinations,

$$g_{LV}^{\nu n} \equiv g_{LV}^{\nu u} + 2g_{LV}^{\nu d} = -\frac{1}{2}, \quad g_{LA}^{\nu n} \equiv g_{LA}^{\nu u} + 2g_{LA}^{\nu d} = -\frac{1}{2}, \quad (73)$$

where $g_{LV}^{\nu n}$ enters proportional to the neutron magnetic moment. $g_{LA}^{\nu n}$ multiplies the CP-violating electric dipole moment operator and can safely be ignored, but the induced pseudoscalar form factor, G_P (which is often neglected), survives even the additional assumption of vanishing second class currents [95]. This

⁷This is consistent with the experimental results of the HAPPEX Collaboration at JLab [90], but since it was necessary to assume the SM values for the EW couplings their analysis cannot be used directly for model independent EW fits. Similar remarks apply to the results by the PVA4 Collaboration at Mainz [91] and the GØ Collaboration at JLab [92]. For recent reviews on parity violation in elastic electron-nucleon scattering with focus on the strangeness content of the nucleon, including more comprehensive lists of references, see Refs. [93,94].

separation also needs full kinematic information, ideally on an event-by-event basis. Ignoring strange quark complications, one could reinterpret the combined value of $\sin^2 \theta_W$ as extracted by the two most precise experiments [96,97] as the constraint, $(g_{LV}^{\nu p})^2 + g_A^2(g_{LA}^{\nu p})^2 = 0.4 \pm 0.1$, but this is only to illustrate the sensitivity. A global analysis including differential cross-sections from ν , $\bar{\nu}$ and e^- elastic and quasi-elastic scattering from both protons and neutrons, and NC and CC channels, may be in order. A very promising future opportunity may be provided by so-called β -beams [98], in which relatively low-energy radioactive nuclei serve as primary neutrino beams. These would allow much better control of the neutrino spectra and one may be able to separate the various form factors kinematically [99].

The isovector axial-vector combination, $\beta \equiv g_{LA}^{\nu u} - g_{LA}^{\nu d} = g_{LA}^{\nu p} - g_{LA}^{\nu n} = 1$ (at the SM tree-level), can be accessed in neutrino induced coherent neutral pion production from nuclei. In the most recent experiment, NOMAD [100] normalized its data to the inclusive CC cross-section, $\sigma(\nu_\mu A \rightarrow \mu^- X)$, which was then taken from their earlier measurement [101]. Comparing the resulting cross-section, $\sigma(\nu_\mu A \rightarrow \nu_\mu A \pi^0)$, to the prediction (based on the PCAC hypothesis) from Ref. [102], we find $\beta^2 = 0.93 \pm 0.14$. The SKAT Collaboration [103] relied only on isospin symmetry when using the NC to CC cross-section ratio,

$$\beta^2 = 2|V_{ud}|^2 \frac{\sigma(\nu_\mu A \rightarrow \nu_\mu A \pi^0)}{\sigma(\nu_\mu A \rightarrow \mu^- A \pi^+)} = 0.93 \pm 0.37. \quad (74)$$

Similarly, the CHARM Collaboration [104] extracted both $\sigma(\nu_\mu A \rightarrow \nu_\mu A \pi^0)$ and $\sigma(\bar{\nu}_\mu A \rightarrow \bar{\nu}_\mu A \pi^0)$, and later measured [105] $\sigma(\nu_\mu A \rightarrow \mu^- A \pi^+)$ and $\sigma(\bar{\nu}_\mu A \rightarrow \mu^+ A \pi^-)$, which we use to derive $\beta^2 = 1.08 \pm 0.54$ and $\beta^2 = 0.93 \pm 0.38$, respectively. Disregarding some older experiments which relied on the same model [102] as NOMAD, we combine these results to obtain $\beta^2 = 0.94 \pm 0.12$.

4.3 Radiative corrections

The leptonic and semileptonic neutrino scattering processes discussed in Sections 4.1 and 4.2 are modified by radiative corrections, which in general depend on energies, experimental cuts, *etc.* This is also true of the Z -pole observables mentioned in Section 3. For those it is conventional to divide the radiative corrections into two classes [15]: one of them consists of QED graphs involving the emission of real photons combined with certain diagrams of virtual photons in loops to form finite and gauge-invariant sets. Photon exchange diagrams, except for vacuum polarization effects, also belong to this class which then needs to be calculated and removed individually for each experiment. On the other hand, purely EW diagrams and associated photonic and gluonic corrections enter EW parameters such as the \bar{g}_V^f and \bar{g}_A^f in Section 3.1, and are considered part of so-called *pseudo-observables* containing the interesting physics. Deviating from these rules, final-state QED and QCD effects (but not initial-final state interference) contributing to the partial and total decay widths of the W and Z bosons are kept.

We now propose a similar strategy where purely EW diagrams and certain photonic loops and γ -exchange graphs are absorbed in the definitions of the low-energy (pseudo-observable) EW couplings, appearing, *e.g.*, in Eqs. (52) and (61). The remaining corrections are assumed to be applied individually for each experiment. However, while the Z -pole pseudo-observables are naturally defined at the scale $\mu = M_Z$, the effective four-Fermi couplings are obtained at momentum transfers $Q^2 \ll M_Z^2$ (even for experiments in the deep-inelastic regime) and the genuine EW radiative corrections will in general depend on the specific kinematic points or ranges at which the low-energy experiments are performed. Thus, one needs to introduce idealized EW coupling parameters defined at some common reference scale μ (we choose $\mu = 0$), and have the experimental collaborations correct for effects due to $Q^2 \neq 0$. The effective NC couplings are modified by the following radiative corrections:

W and Z boson self-energies: Fermion and W boson bubbles inserted into the Z boson propagator are to be evaluated at $Q^2 = 0$ and subtracted from the analogous corrections to the W propagator. This results in the most important contribution to the universal low-energy ρ parameter defined in

the second Eq. (47). ρ also contains vertex and WZ box⁸ corrections to the μ -lifetime from which G_F in Eq. (13) was obtained and in terms of which the low-energy Lagrangians are normalized.

γ - Z mixing: Vacuum polarization diagrams of γ - Z mixing type give rise to a scale-dependence [18] of the weak mixing angle (see Figure 1). In the perturbative QCD domain, $\mu \gtrsim 1$ GeV, these effects can be re-summed [17], while the non-perturbative region introduces a hadronic uncertainty which is, however, small compared to the current and foreseeable experimental precision [3,17]. Here we employ the weak mixing angle at the reference scale $\mu = 0$ and abbreviate, $\hat{s}_0^2 \equiv \sin^2 \theta_W(0)$.

Neutrino charge radius: The charge radius of the ℓ -neutrino, $\not\partial_{\nu_\ell W}$, is generated by a loop insertion into the ν_ℓ -line consisting of a W boson and the charged lepton ℓ (in most cases $\nu_\ell = \nu_\mu$). Attaching the photon to the W boson produces a simple universal correction. By contrast, attaching it to the lepton ℓ generates a large EW logarithm, which is regulated at m_ℓ . This allows photon exchange diagrams connecting $\not\partial_{\nu_\ell W}$ with the target fermion.

WW and ZZ box diagrams: The left-handed couplings $g_{LL}^{\nu_e}$ and $g_{LL}^{\nu_d}$ receive a contribution from the WW box, \square_{WW} , and $g_{LL}^{\nu_u}$ from the WW crossed-box, Σ_{WW} . In addition, the effective couplings of either chirality, $g_{LX}^{\nu f}$, get a correction term proportional to $(g_{LX}^{\nu f})^2$ from the sum of both types of ZZ box diagrams, \boxtimes_{ZZ} , in which $(g_{LX}^{\nu f})^2$ is evaluated at lowest order, but replacing \hat{s}_0^2 by \hat{s}_Z^2 .

Collecting these corrections [106] one obtains,

$$g_{LL}^{\nu_e f} = \rho \left[\frac{1}{2} - Q_f \hat{s}_0^2 + \boxtimes_{ZZ} \right] - Q_f \not\partial_{\nu_\ell W} + \Sigma_{WW} \quad (f = u), \quad (75)$$

$$g_{LL}^{\nu_e f} = \rho \left[-\frac{1}{2} - Q_f \hat{s}_0^2 + \boxtimes_{ZZ} \right] - Q_f \not\partial_{\nu_\ell W} + \square_{WW} \quad (f = d, e), \quad (76)$$

$$g_{LR}^{\nu_e f} = -\rho [Q_f \hat{s}_0^2 + \boxtimes_{ZZ}] - Q_f \not\partial_{\nu_\ell W} \quad (f = u, d, e), \quad (77)$$

where

$$\not\partial_{\nu_\ell W} = -\frac{\alpha}{6\pi} \left(\ln \frac{M_W^2}{m_\ell^2} + \frac{3}{2} \right), \quad (78)$$

$$\square_{WW} = -\frac{\hat{\alpha}_Z}{2\pi \hat{s}_Z^2} \left[1 - \frac{\hat{\alpha}_s(M_W)}{2\pi} \right], \quad \Sigma_{WW} = \frac{\hat{\alpha}_Z}{8\pi \hat{s}_Z^2} \left[1 + \frac{\hat{\alpha}_s(M_W)}{\pi} \right], \quad (79)$$

$$\boxtimes_{ZZ} = -\frac{3\hat{\alpha}_Z}{8\pi \hat{s}_Z^2 \hat{c}_Z^2} (g_{LX}^{\nu_e f})^2 \left[1 - \frac{\hat{\alpha}_s(M_Z)}{\pi} \right]. \quad (80)$$

For the numerical SM evaluation we assume $M_H = 125.5$ GeV (see Section 3.3) yielding,

$$\rho = 1.00064, \quad \hat{s}_0^2 = 0.23865, \quad \hat{s}_Z^2 = 0.23126, \quad \hat{\alpha}_Z^{-1} = 127.94, \quad (81)$$

and with that we find the SM values in Table 6. We also give the results for the combinations,

$$g_L^2 = 0.3034, \quad h_L^2 = -0.0643, \quad g_R^2 = 0.0302, \quad h_R^2 = 0.0181, \quad (82)$$

$$\tan \theta_L \equiv \frac{g_{LL}^{\nu_\mu u}}{g_{LL}^{\nu_\mu d}} = -0.8062, \quad \tan \theta_R \equiv \frac{g_{LR}^{\nu_\mu u}}{g_{LR}^{\nu_\mu d}} = -2 + \frac{3\hat{\alpha}_Z}{4\pi \hat{c}_Z^2} \left(1 - \frac{\hat{\alpha}_s}{\pi} \right) = -1.9977, \quad (83)$$

where the explicit expression for $\tan \theta_R$ is exact to one-loop order, with $\tan \theta_R \neq -2$ entirely due to the ZZ box diagrams. Similarly, $\beta^2 = 1.0151$, where $\beta^2 \neq 1$ is mostly due to the WW box diagrams. The

Table 6: SM values of the one-loop and leading two-loop corrected effective NC ν couplings for the charged SM fermions and the nucleons. Note, that the small $g_{LR}^{\nu\mu n}$ arises solely from the ZZ box diagrams.

f	e	u	d	p	n
$g_{LL}^{\nu\mu f}$	-0.2730	0.3457	-0.4288	0.2626	-0.5119
$g_{LR}^{\nu\mu f}$	0.2334	-0.1553	0.0777	-0.2328	0.0002
$g_{LV}^{\nu\mu f}$	-0.0396	0.1905	-0.3511	0.0298	-0.5117
$g_{LA}^{\nu\mu f}$	-0.5064	0.5010	-0.5065	0.4955	-0.5121

parameters $\theta_{L,R}$ are useful because together with $g_{L,R}^2$ they form a parameter set with small correlations when it is extracted from the current data, while the $g_{LL}^{\nu\mu q}$ and $g_{LR}^{\nu\mu q}$ have non-Gaussian errors.

Under realistic conditions one has to correct the $g_{LV}^{\nu\mu f}$ for $Q^2 \neq 0$ (the $g_{LA}^{\nu\mu f}$ are Q^2 -independent). In the case of ν_μ - e scattering with energies $E_{\nu_\mu} \lesssim 100$ GeV, the resulting values of $Q^2 \lesssim m_\mu^2$ hardly affect $\varnothing_{\nu_\mu W}$, and the correction to \hat{s}^2 is suppressed by a factor $(1 - 4\hat{s}_0^2) \ll 1$, so that the residual Q^2 -correction is two orders of magnitude below the experimental uncertainty in Table 4. The average Q^2 of most ν DIS experiments is around the bottom quark and τ lepton thresholds so that we can write,

$$g_{LV}^{\nu\mu q} \rightarrow g_{LV}^{\nu\mu q} - 2Q_q \left[\hat{s}_Q^2 - \hat{s}_0^2 + \frac{\alpha}{6\pi} \left(\ln \frac{Q^2}{m_\mu^2} + 5 - \frac{160}{9} \hat{s}_0^2 + \Delta_Q^{\nu\mu q} \right) \right] \approx g_{LV}^{\nu\mu q} + 0.0005 Q_q \ln \frac{Q^2}{2.2 \text{ GeV}^2}, \quad (84)$$

where $\hat{s}_Q^2 \equiv \sin^2 \hat{\theta}_W(Q^2)$, and where significant cancellations occur between the Q^2 -variations of $\sin^2 \hat{\theta}_W$ and $\varnothing_{\nu_\mu W}$. The small Q^2 -dependent correction term $\Delta_Q^{\nu\mu q}$ accounts for non-decoupling bottom and τ effects, the non-vanishing masses of the lighter fermions, and some reducible higher-order contributions.

5 Parity Violation

5.1 Parity-violating Møller scattering

The parity-violating part of the electron-electron interaction is to leading order a purely weak NC process. From the second Eq. (25) one finds,

$$\mathcal{L}_{\text{NC}}^{ee} = -\frac{\cos^2 \theta_W}{v^2} \bar{e} \gamma^\mu \frac{g_V^e - g_A^e \gamma^5}{2} e \bar{e} \gamma_\mu \frac{g_V^e - g_A^e \gamma^5}{2} e = -\frac{1}{v^2} \bar{e} \gamma^\mu \frac{g_{VV}^{ee} e \bar{e} - g_{AA}^{ee} \gamma^5 e \bar{e} \gamma^5 + 2g_{VA}^{ee} e \bar{e} \gamma^5}{4} \gamma_\mu e, \quad (85)$$

where the SM tree-level relations for the coefficients multiplying parity-conserving four-Fermi operators are,

$$g_{VV}^{ee} \equiv (\cos \theta_W g_V^e)^2 = \frac{(1 - 4 \sin^2 \theta_W)^2}{2}, \quad g_{AA}^{ee} \equiv (\cos \theta_W g_A^e)^2 = \frac{1}{2}, \quad (86)$$

while for parity-violating processes one has,

$$g_{VA}^{ee} = \cos^2 \theta_W g_V^e g_A^e \equiv \cos^2 \theta_W (g_L^e{}^2 - g_R^e{}^2) = \frac{1}{2} - 2 \sin^2 \theta_W. \quad (87)$$

⁸The $W\gamma$ box has been removed as it is part of the traditional QED correction to μ -decay within the $V - A$ theory [38].

g_{VA}^{ee} can be measured in fixed target polarized Møller scattering, $\bar{e}^-e^- \rightarrow e^-e^-$, by observing the left-right cross-section asymmetry [107], A_{LR}^{ee} , which — to an excellent approximation — reduces to the interference term of the parity-violating part of the EW amplitude with the parity-conserving QED amplitude. For large incident electron energies, $E_e \gg m_e$, it can be written as,

$$A_{LR}^{ee} \equiv \frac{d\sigma_L - d\sigma_R}{d\sigma_L + d\sigma_R} = 2 \frac{s}{M_Z^2} \frac{g_L^e{}^2 - g_R^e{}^2}{(2Q_A^e)^2} \mathcal{F}^{ee} = \frac{2m_e E_e}{v^2} \frac{g_{VA}^{ee}}{4\pi\alpha} \mathcal{F}^{ee} \approx \frac{s}{M_Z^2} \left[\frac{1}{\sin^2 2\theta_W} - \frac{1}{\cos^2 \theta_W} \right] \frac{\mathcal{F}^{ee}}{2}, \quad (88)$$

where $s = 2m_e E_e$ is the square of the center-of-mass energy, y is again the relative energy transfer, and

$$\mathcal{F}^{ee} \equiv \mathcal{F}^{ee}(Q^2, y) = \frac{2y(1-y)}{(1-y+y^2)^2} \mathcal{F}_{\text{QED}}^{ee}(Q^2, y) = \frac{4y(1-y)}{1+y^4+(1-y)^4} \mathcal{F}_{\text{QED}}^{ee}(Q^2, y). \quad (89)$$

The QED radiative correction factor, $\mathcal{F}_{\text{QED}}(Q^2, y)$, includes kinematically weighted hard initial and final state radiation effects, the $\gamma\gamma$ box graphs, and the non-logarithmic contributions from the charge radius and the γZ box diagrams [108,109]. A_{LR}^{ee} has been obtained at $y = 0.6$ and at low $Q^2 = ys = 0.026 \text{ GeV}^2$ in the SLAC-E158 experiment [59] using the 89% polarized e^- beam of the SLC, with the result,

$$A_{LR}^{ee} = (1.31 \pm 0.14_{\text{stat.}} \pm 0.10_{\text{syst.}}) \times 10^{-7}. \quad (90)$$

For the conditions⁹ of the experiment at the SLC one obtains $\mathcal{F}_{\text{QED}}(0.026 \text{ GeV}^2, 0.6) = 1.01 \pm 0.01$ and $F^{ee}(0.026 \text{ GeV}^2, 0.6) \approx 0.84$, and anticipating the first correction (119) in Section 5.4 we can extract,

$$g_{VA}^{ee} = 0.0190 \pm 0.0027, \quad (91)$$

which is 1.3σ below the SM prediction of $g_{VA}^{ee} = 0.0225$. Expressed in terms of the weak mixing angle in the $\overline{\text{MS}}$ -scheme, Eq. (91) yields,

$$\hat{s}^2(0.16 \text{ GeV}) = 0.2403 \pm 0.0013, \quad (92)$$

and establishes the scale dependence of the weak mixing angle (see Figure 1) at the level of 6.4 standard deviations. The implications for physics beyond the SM are discussed in Refs. [3,18,111].

A new and five times more precise experiment [112] of this type is planned at Jefferson Laboratory (JLab) at the 11 GeV upgraded CEBAF. The kinematics will be at $y \approx 0.57$ and $Q^2 \approx 0.0056 \text{ GeV}^2$, giving an even smaller asymmetry. As shown in Figure 8, this experiment will provide one of the most precise determinations of $\sin^2 \theta_W$ and the most precise one off the Z pole, and will have important implications for the indirect determination of M_H .

5.2 Parity non-conservation in atoms and ions

The parity-violating part of the NC electron-quark interactions is described by the Lagrangian,

$$\mathcal{L}_{\text{NC}}^{eq} = -\frac{2}{v^2} \frac{\bar{e}\gamma^5\gamma^\mu e}{2} \left[g_{AV}^{eu} \frac{\bar{u}\gamma_\mu u}{2} + g_{AV}^{ed} \frac{\bar{d}\gamma_\mu d}{2} \right] - \frac{2}{v^2} \frac{\bar{e}\gamma^\mu e}{2} \left[g_{VA}^{eu} \frac{\bar{u}\gamma^5\gamma_\mu u}{2} + g_{VA}^{ed} \frac{\bar{d}\gamma^5\gamma_\mu d}{2} \right], \quad (93)$$

where the SM tree-level relations for the real-valued coefficients g_{AV}^{eq} and g_{VA}^{eq} ,

$$g_{AV}^{eu} \equiv \cos^2 \theta_W g_A^e g_V^u = -\frac{1}{2} + \frac{4}{3} \sin^2 \theta_W, \quad g_{AV}^{ed} \equiv \cos^2 \theta_W g_A^e g_V^d = \frac{1}{2} - \frac{2}{3} \sin^2 \theta_W, \quad (94)$$

⁹The numerical values for y and Q^2 are effective quantities defined to match the analyzing power obtained from a Monte Carlo simulation which accounts for energy losses in the target, *etc.*, and are not identical to the nominal ones. Note, that even though the analyzing power is proportional to $\alpha^{-1}(Q^2)$ [59] we used instead α^{-1} in Eq. (88) because the Q^2 -dependence due to lepton loops cancels exactly between $\sin^2 \theta_W$ in g_{VA}^{ee} and α , while hadronic loops are negligible [110].

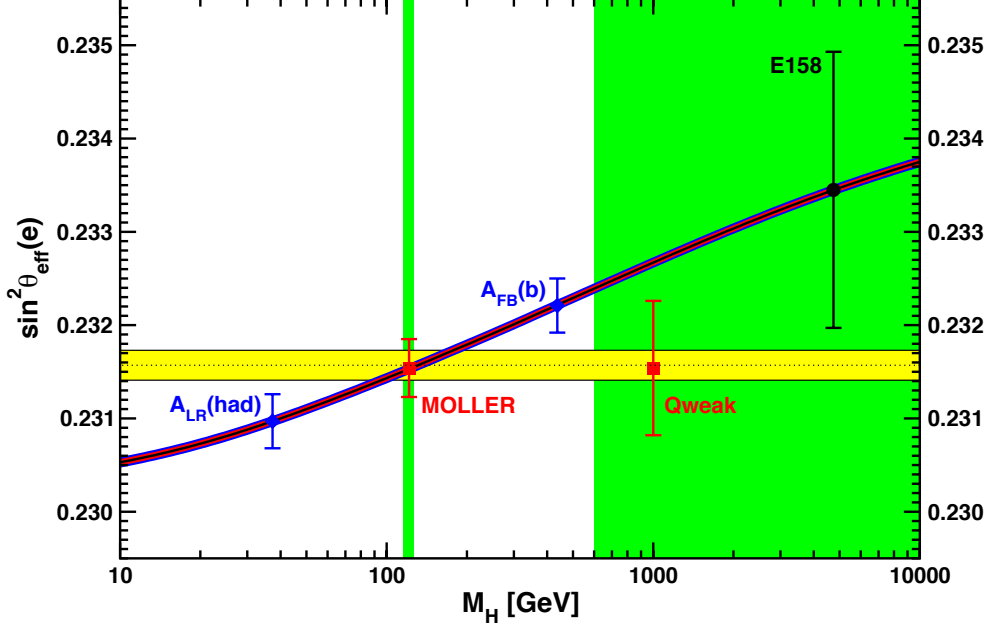


Figure 8: High precision measurements of $\sin^2 \theta_{\text{eff}}^\ell$. Shown in blue are the most precise Z -pole values and in black the presently most precise low-energy determination [59]. Projections for two of the future experiments are shown in red. See the body of the text for more details.

$$g_{VA}^{eu} \equiv \cos^2 \theta_W g_V^e g_A^u = -\frac{1}{2} + 2 \sin^2 \theta_W, \quad g_{VA}^{ed} \equiv \cos^2 \theta_W g_V^e g_A^d = \frac{1}{2} - 2 \sin^2 \theta_W, \quad (95)$$

coincide with the similarly defined effective couplings, C_{1q} and C_{2q} , respectively. These interactions induce extremely small parity-violating effects in atomic physics [113,114] which grow roughly with the third power of atomic number, Z , and atomic parity violation (APV) has been observed only in heavy atoms, such as cesium [115,116] and thallium [117,118]. In order to interpret these effects in terms of the interactions (93) one also needs a good understanding of atomic structure [119,120]. This has been achieved for ^{133}Cs [121,122], the nucleus where also the greatest experimental precision was obtained [115]. The effective couplings in Eq. (94) add up coherently across the nucleus and give rise to the nuclear spin-independent interaction. It can be isolated from the much smaller spin-dependent interaction by measuring different hyperfine transitions. However, the couplings in Eq. (95) are clouded by the nuclear anapole moment [123,124], which grows as $Z^{2/3}$ and dominates in heavy nuclei.

The EW physics is contained in the nuclear weak charges which are defined by,

$$Q_W^{Z,N} \equiv -2 [Z(g_{AV}^{ep} + 0.00005) + N(g_{AV}^{en} + 0.00006)] \left(1 - \frac{\alpha}{2\pi}\right) \approx Z(1 - 4 \sin^2 \theta_W) - N, \quad (96)$$

where N is the number of neutrons in the nucleus, and where the nucleon couplings are given by,

$$g_{AV}^{ep} \equiv 2g_{AV}^{eu} + g_{AV}^{ed} = -\frac{1}{2} + 2 \sin^2 \theta_W, \quad g_{AV}^{en} \equiv g_{AV}^{eu} + 2g_{AV}^{ed} = \frac{1}{2}. \quad (97)$$

The small numerical adjustments in Eq. (96) are discussed in Section 5.4. *E.g.*, the weak charge of ^{133}Cs , $Q_W^{55,78}$, is extracted by measuring experimentally the ratio of the parity-violating amplitude, E_{PNC} , to

the Stark vector transition polarizability, β , and by calculating E_{PNC} theoretically in terms of $Q_W^{55,78}$,

$$Q_W^{Z,N} = N \left(\frac{\text{Im } E_{\text{PNC}}}{\beta} \right)_{\text{exp.}} \left(\frac{Q_W^{Z,N}}{N \text{Im } E_{\text{PNC}}} \right)_{\text{th.}} \beta_{\text{exp.+th.}} \approx 2(N-Z) \left[\frac{1}{2} + \frac{2Z}{N-Z} \sin^2 \theta_W \right]. \quad (98)$$

Notice, the reduced sensitivity to $\sin^2 \theta_W$. The ratio of the off-diagonal hyperfine amplitude to the polarizability was measured directly by the Boulder group [125]. Combined with the precisely known hyperfine amplitude [126] one extracts the value $\beta = (26.991 \pm 0.046) a_B^3$, where a_B is the Bohr radius. A recent state-of-the-art many body calculation [121] yields,

$$\text{Im } E_{\text{PNC}} = (0.8906 \pm 0.0026) \times 10^{-11} |e| a_B \frac{Q_W^{Z,N}}{N}, \quad (99)$$

while the two measurements [115,116] combine to give $\text{Im } E_{\text{PNC}}/\beta = -(1.5924 \pm 0.0055) \text{ mV/cm}$, or if β is given in atomic units as is adequate for Eq. (98), $\text{Im } E_{\text{PNC}}/\beta = -(3.0967 \pm 0.0107) \times 10^{-13} |e|/a_B^2$. We finally obtain $Q_W^{55,78} = -73.20 \pm 0.35$, and by virtue of Eq. (96),

$$55g_{AV}^{ep} + 78g_{AV}^{en} = 36.64 \pm 0.18, \quad (100)$$

in excellent agreement with the SM prediction, $55g_{AV}^{ep} + 78g_{AV}^{en} = 36.66$. However, a very recent atomic structure calculation [122] found significant corrections to two non-dominating terms, shifting the numerical coefficient in Eq. (99) to $(0.8977 \pm 0.0040) \times 10^{-11}$, and yielding in place of Eq. (100) the constraint, $55g_{AV}^{ep} + 78g_{AV}^{en} = 36.35 \pm 0.21$ ($Q_W^{55,78} = -72.62 \pm 0.43$), a 1.5σ SM deviation [122].

The theoretical uncertainties are 3% for thallium [127] but larger for other atoms. In the future it could be possible to reduce the theoretical wave function uncertainties by taking ratios of parity violation in different isotopes [113,128]. There would still be some residual uncertainties [129,130] from differences in the *neutron skin* (the excess of the root-mean-square radii of the neutron over the proton distributions), however. This is because the atomic wave function for *s*-states is maximal at the origin so that a broader neutron distribution results in a smaller overall effect (the neutron weak charge dominates over that of the proton). Incidentally, the neutron skin may also affect APV in single isotopes [131]. It has recently been observed in polarized electron scattering from ^{208}Pb by the PREX Collaboration [132]. Note also, that unlike single isotopes, the isotope ratios constrain mostly new physics contributions to g_{AV}^{ep} [133]. Experiments in hydrogen and deuterium are another possibility for reducing the atomic theory uncertainties [134], while measurements of trapped radioactive atoms [135] (most notably francium) and single trapped radium ions are promising [136] because of the much larger parity-violating effects.

5.3 Parity-violating deep-inelastic scattering and related processes

In an experiment similar to the process discussed in Section 5.1 and at about the same Q^2 , the Qweak Collaboration at JLab [137] has completed data taking to determine,

$$A_{LR}^{ep} \equiv \frac{d\sigma_L - d\sigma_R}{d\sigma_L + d\sigma_R} = 2 \frac{s}{M_Z^2} \frac{g_A^e(2g_V^u + g_V^d)}{4Q_A^e(2Q_A^u + Q_A^d)} \mathcal{F}^{ep} = -\frac{m_p(2E_e + m_p)}{v^2} \frac{g_{AV}^{ep}}{4\pi\alpha} \mathcal{F}^{ep}, \quad (101)$$

in elastic 85% polarized ep scattering, $\vec{e}^- p \rightarrow e^- p$, where $s = m_p(2E_e + m_p)$ for $m_e \ll E_e$, and

$$\mathcal{F}^{ep} \equiv \mathcal{F}^{ep}(Q^2, y) = [y + \mathcal{O}(y^2)] \mathcal{F}_{\text{QED}}^{ep}(Q^2, y). \quad (102)$$

A beam energy of 1.165 GeV at a nominal scattering angle of $\theta_{\text{lab}} = 7.9^\circ$ keeps both $Q^2 = 0.026 \text{ GeV}^2$ and $y \approx 0.0085$ perturbatively small. This is necessary because the $\mathcal{O}(y^2)$ -term in Eq. (102) is plagued

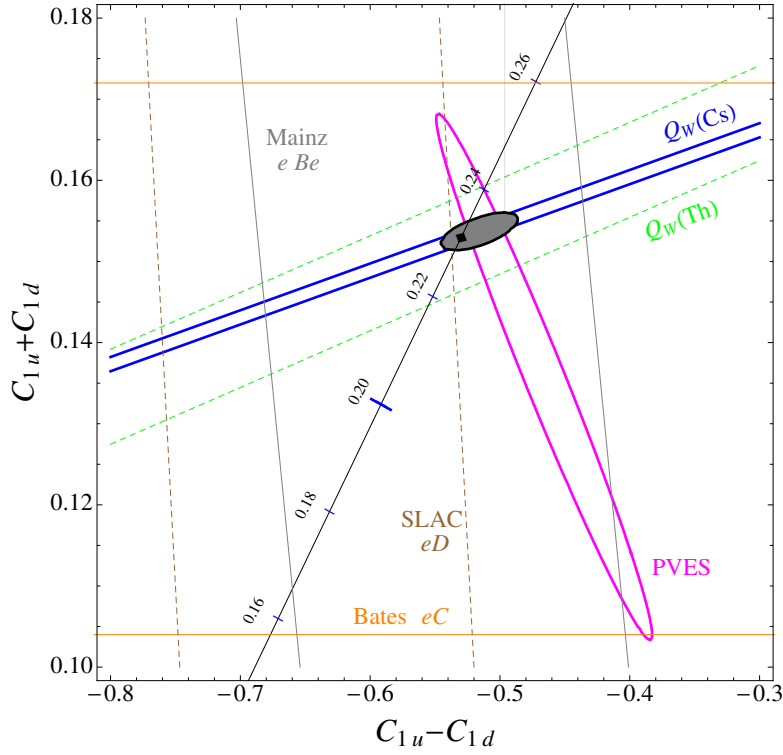


Figure 9: Constraints on the effective NC couplings, C_{1u} and C_{1d} , from recent (PVES) and older parity-violating electron scattering, and from APV at 1σ , as well as the 90% CL global best fit (shaded) and the SM prediction as a function of the weak mixing angle \hat{s}_Z^2 . The SM best fit value $\hat{s}_Z^2 = 0.23116$ is also indicated. (Figure reprinted as permitted according to journal guidelines from *Phys. Rev. D* 86 (2012) 010001, J. Erler and P. Langacker [15].)

by large hadronic uncertainties and must be kept below the experimental error. It is precisely the option to restrict to forward angles which makes this kind of measurement possible in elastic \bar{e}^- but not ν scattering (see the discussion in Section 4.2). In practice, an extrapolation to $y \rightarrow 0$ will be performed using other asymmetry measurements [93] in parity-violating electron scattering (PVES) at higher Q^2 -values (see Figure 9). Overall, the SM prediction, $A_{LR}^{ep} = 265$ ppb, at Q_{weak} is comparable to A_{LR}^{ee} at E158. The additional experiment specific corrections (117) and (118) to g_{AV}^{ep} discussed in Section 5.4 are sometimes absorbed together with the axial current renormalization into the weak charge of the proton,

$$Q_W^p \equiv -2(g_{AV}^{ep} - 0.0021 - 0.0004) \left(1 - \frac{\alpha}{2\pi}\right) \approx 1 - 4\sin^2\theta_W. \quad (103)$$

The anticipated experimental precision is 2.5% for A_{LR}^{ep} , but due to the hadronic dilution (the $\mathcal{O}(y^2)$ -term contributes about one third to A_{LR}^{ep}), as well as the uncertainty (1.5%) from the proton structure, it is larger (4.1%) for Q_W^p . Including the current estimate of the additional hadronic γZ box dilution and its uncertainty in Eq. (117) results in a 4.5% or ± 0.0016 error in g_{AV}^{ep} , which in turn would allow for a ± 0.0008 determination of $\sin^2\theta_W$. We note that following the appearance of Ref. [138] the γZ box contribution has been subjected to considerable theoretical scrutiny (see the discussion and references in Section 5.4). It will be important to perform additional experiments, in particular in parity-violating structure functions at low Q^2 , such as those planned at JLab, which can constrain the associated dispersion integrals. The implications for new physics are discussed in Ref. [111].

Both types of hadronic dilutions and uncertainties will be significantly smaller at a similar experiment proposed at Mainz [139] with a lower beam energy of 200 MeV and $Q^2 = 0.0048 \text{ GeV}^2$ (at $\theta_{\text{lab}} = 20^\circ$).

With these parameters a precision of 1.7% in A_{LR}^{ep} and 2% in g_{AV}^{ep} may be feasible, *i.e.*, an extraction of $\sin^2 \theta_W$ with ± 0.00036 accuracy. A precise measurement of the model-independent coupling g_{AV}^{ep} would also greatly reduce the allowed parameter space in the C_{1q} (g_{AV}^{eq}) plane shown in Figure 9.

The coherent sum of couplings, $g_{AV}^{eu} + g_{AV}^{ed}$, can be extracted by elastic scattering off isoscalar nuclei. The asymmetry has been measured at MIT-Bates to 25% using a ^{12}C target [140]. A much more precise determination would be very interesting as it would over-constrain the parameter space in Figure 9.

On the other hand, the C_{2q} (g_{VA}^{eq}) are harder to come by. Experiments in parity-violating deep-inelastic scattering [141] are sensitive to the interference of the quark-level amplitudes corresponding to $\mathcal{L}_{\text{NC}}^{eq}$ with the QED amplitudes. Scattering from an isoscalar target provides information on the charge weighted combinations, $2g_{AV}^{eu} - g_{AV}^{ed}$ and $2g_{VA}^{eu} - g_{VA}^{ed}$. Specifically, in the simple quark model and in the limit of vanishing m_p ,

$$A_{LR}^{\text{eDIS}} \equiv 2 \frac{sy}{M_Z^2} \frac{g_A^e \sum_q Q_A^q g_V^q [q(x) + \bar{q}(x)] [1 + (1-y)^2] + g_V^e \sum_q Q_A^q g_A^q [q(x) - \bar{q}(x)] [1 - (1-y)^2]}{Q_A^e \sum_q (2Q_A^q)^2 [q(x) + \bar{q}(x)] [1 + (1-y)^2]} \approx -\frac{9}{20\pi\alpha(Q)} \frac{Q^2}{v^2} \left[\left(\frac{2}{3} g_{AV}^{eu} - \frac{1}{3} g_{AV}^{ed} \right) + \left(\frac{2}{3} g_{VA}^{eu} - \frac{1}{3} g_{VA}^{ed} \right) \frac{1 - (1-y)^2}{1 + (1-y)^2} \right], \quad (104)$$

where the last expression is the valence quark approximation, which should be reasonable at larger values of $x \gtrsim 0.4$. One has to correct for higher twist effects (especially at low Q^2 and high $x \gtrsim 0.5$), charge symmetry violations (expected to grow with x), quark-quark correlations, sea quark contributions, target mass effects, longitudinal structure functions and nuclear effects [3] (see also Section 4.2). These effects should not exclusively be seen as limitations, but are of considerable interest in their own right.

Because of the larger values of $Q^2 \gtrsim 1 \text{ GeV}$ in eDIS experiments, and also due to the absence of the $1 - 4\sin^2 \theta_W$ suppression, the asymmetry in Eq. (104) is much larger ($\gtrsim 10^{-4}$) than the asymmetries measured in elastic scattering. It has been obtained to about 10% precision at SLAC [142] in a Q^2 range between 0.92 and 1.96 GeV^2 , and $0.15 \leq y \leq 0.36$, providing a 7% determination of $\sin^2 \theta_W$ and clarifying the confused situation regarding the SM which prevailed at the time. Two further data points have been collected [143] at $Q^2 = 1.1 \text{ GeV}^2$ and $Q^2 = 1.9 \text{ GeV}^2$ at the 6 GeV CEBAF, each with about 2.5% precision. The Collaboration is currently analyzing the data. A large array of data points will be taken [144] after the CEBAF upgrade to 11 GeV. The kinematic ranges will be between 1.9 and 9.5 GeV^2 and $0.2 \lesssim x \lesssim 0.7$ (mostly around $y \approx 0.7$). These broad ranges will allow to separate the EW physics from the strong interaction issues and it is hoped to extract the bracketed linear combination of couplings on the r.h.s. of Eq. (104) to 0.5% accuracy, and $\sin^2 \theta_W$ with an uncertainty of ± 0.0006 .

An experiment at CERN [145] obtained a different kind of DIS asymmetry by reversing the charge of projectile muons simultaneously with the helicity (the reversals occurred every 6 days rather than in fractions of seconds as in eDIS). Since reversing the helicity of muons is much more difficult, the precision ($\approx 25\%$) was rather poor. But this is the only experiment in which the P -even, C -odd couplings,

$$g_{AA}^{eu} \equiv \cos^2 \theta_W g_A^e g_A^u = -\frac{1}{2}, \quad g_{AA}^{ed} \equiv \cos^2 \theta_W g_A^e g_A^d = \frac{1}{2}, \quad (105)$$

entered into the equations (in the combination $2g_{AA}^{eu} - g_{AA}^{ed}$) in addition to $2g_{VA}^{eu} - g_{VA}^{ed}$.

Another possibility to find information on the g_{VA}^{eq} couplings is through elastic or quasi-elastic scattering experiments at backward angles. They enter through the axial-vector form factor, G_A^e (see, *e.g.*, Ref. [146]), which becomes dominant in the backward direction. Unfortunately, somewhat paralleling the discussion in Section 4.2, the strange quark contribution, $\Delta\mu_s$, to the magnetic moment of the nucleon, as well as the nucleon anapole moment (a weak interaction effect between two different quarks in the nucleon, in analogy to the nuclear anapole moment mentioned in Section 5.2) are obstructions to a clean determination. Moreover, according to Eqs. (95) the isoscalar coupling, $g_{VA}^{eu} + g_{VA}^{ed}$, vanishes to lowest order and is usually set to zero, while the focus is on the isovector combination, $g_{VA}^{eu} - g_{VA}^{ed}$. Experimental results are available for scattering from hydrogen [147], deuterium [148], and ^9B [149].

5.4 Radiative corrections

The inclusion of EW radiative corrections to the NC effective couplings accessible in parity-violating low-energy observables follows closely the discussion in Section 4.3. In particular, the W and Z boson self-energy corrections and the related contributions to the ρ parameter, as well as the γ - Z mixing renormalization effects [17,18] are the same. The results from the WW and ZZ boxes also carry over. However, the following comments are in order:

Electron and quark charge radii: Both W and Z bosons contribute to the EW charge radii of charged fermions. The $g_{AV}^{\ell f}$ couplings receive large EW logarithms from the Z loop contribution to the charge radii of charged leptons, $\delta_{\ell Z}$. The logarithms entering the quark charge radii, δ_{qW} and δ_{qZ} , are regulated at the strong interaction scale, introducing a hadronic theory uncertainty into the $g_{VA}^{\ell q}$ unless they are extracted in the perturbative QCD regime of DIS. For definiteness we choose for the quark mass $m_q = m_p$ in the low-energy parton model expression. The δ_{fZ} are proportional to the vector couplings of fermion f which introduce additional dependences on $\sin \hat{\theta}_W(\mu)$, and so μ needs to be chosen appropriately. We take $\mu^2 = m_f M_Z$ for the low-energy couplings, and in the absence of a two-loop calculation, we postulate that more generally $\mu^2 = \sqrt{Q^2} M_Z$ will provide a good approximation at least when $Q^2 \gg m_f^2$. Analogous remarks apply to the vector couplings entering through the γZ box graphs discussed next.

γZ box diagrams: A new feature compared to the ν case is the appearance of γZ box, $\boxtimes_{\gamma Z}$, graphs¹⁰ generating large logarithms in both $g_{VA}^{\ell q}$ and $g_{AV}^{\ell q}$. As before we regulate the parton model result at $m_q = m_p$, while the full effect depends on kinematical details. Indeed, the $\boxtimes_{\gamma Z}$ terms entering the $g_{AV}^{\ell q}$ are suppressed by a factor $(1 - 4 \sin^2 \hat{\theta}_W)$ when they are extracted from APV [150] but for the conditions of polarized electron scattering [138] there is an admixture of the $\boxtimes'_{\gamma Z}$ structure (see below) where this suppression is lifted. Again we propose to correct for these experiment dependent effects relative to the choice $m_q = m_p$.

Two-loop QCD corrections: g_{AV}^{ep} is suppressed by a factor $(1 - 4\hat{s}_0^2)$ but the WW box contributions are not. Rather they are further enhanced by an additional factor of 7 compared to g_{AV}^{ee} , resulting in a loop effect similar in size as the tree-level result and perturbative QCD corrections to the EW box [111] should be included.

Axial current renormalization: In the original work on radiative corrections to APV [150] the authors included QED renormalization terms at $q^2 = 0$, multiplying each axial current vertex, $Z_\mu \bar{f} \gamma^\mu \gamma^5 f$, by a factor $(1 - Q_f^2 \alpha / 2\pi)$. However, the analogous QCD renormalization of the axial vertices of quarks, which cannot be computed perturbatively at small q^2 , has been omitted. Even the term at the free electron vertex should in principle be recalculated for bound state electrons in heavy atoms [151]. In any case, consistent with the general strategy proposed in Section 4.3, QED and QCD corrections to external lines are not considered as part of the EW couplings, and in fact have not been added in the neutrino scattering case [106]. We therefore *remove* these small terms ($\lesssim 0.1\%$) from the effective NC couplings in the present case as well, with the understanding that they are being accounted for together with the other remaining radiative corrections.

Collecting these corrections [110,111,150,152],

$$g_{AV}^{\ell f} = \rho \left[-\frac{1}{2} + 2 Q_f \hat{s}_0^2 - 2 Q_f \delta_{\ell Z} + \boxtimes_{ZZ} + \boxtimes_{\gamma Z} \right] - 2 Q_f \delta_{\ell W} + \square_{WW} \quad (f = u), \quad (106)$$

¹⁰The interference of $\gamma\gamma$ box diagrams with single γ or Z exchanges also enters at this perturbative order but this does not affect the NC amplitudes or effective Lagrangians such as in Eq. (85), so we do not consider them here.

$$g_{AV}^{\ell f} = \rho \left[\frac{1}{2} + 2Q_f \hat{s}_0^2 - 2Q_f \not{\partial}_{\ell Z} + \boxtimes_{ZZ} + \boxtimes_{\gamma Z} \right] - 2Q_f \not{\partial}_{\ell W} + \mathbb{X}_{WW} \quad (f = d, e), \quad (107)$$

$$g_{VA}^{\ell u} = \rho \left[-\frac{1}{2} + 2\hat{s}_0^2 + 2\not{\partial}_{uZ} + \boxtimes'_{ZZ} + \boxtimes'_{\gamma Z} \right] + 2\not{\partial}_{uW} + \square_{WW}, \quad (108)$$

$$g_{VA}^{\ell d} = \rho \left[\frac{1}{2} - 2\hat{s}_0^2 + 2\not{\partial}_{dZ} + \boxtimes'_{ZZ} + \boxtimes'_{\gamma Z} \right] + 2\not{\partial}_{dW} + \mathbb{X}_{WW}, \quad (109)$$

where using the abbreviation, $\hat{\alpha}_{ij} \equiv \hat{\alpha}(\sqrt{m_i M_j})$, we defined,

$$\not{\partial}_{\ell W} = \frac{2\alpha}{9\pi}, \quad \not{\partial}_{uW} = -\frac{\alpha}{18\pi} \left(\ln \frac{M_W^2}{m_p^2} + \frac{25}{6} \right), \quad \not{\partial}_{dW} = \frac{\alpha}{9\pi} \left(\ln \frac{M_W^2}{m_p^2} + \frac{13}{6} \right), \quad (110)$$

$$\not{\partial}_{fZ} = \frac{\alpha}{6\pi} Q_f g_{VA}^{ff} \left(\ln \frac{M_Z^2}{m_f^2} + \frac{1}{6} \right), \quad (111)$$

and,

$$\boxtimes_{ZZ} = -\frac{3\hat{\alpha}_Z}{16\pi \hat{s}_Z^2 \hat{c}_Z^2} \left(g_{VA}^{\ell f} g_{VV}^{\ell f} + g_{AV}^{\ell f} g_{AA}^{\ell f} \right) \left[1 - \frac{\hat{\alpha}_s(M_Z)}{\pi} \right], \quad (112)$$

while \boxtimes'_{ZZ} is given by \boxtimes_{ZZ} with $g_{VA}^{\ell f} \leftrightarrow g_{AV}^{\ell f}$, and \square_{WW} and \mathbb{X}_{WW} are defined in Eqs. (79). Furthermore,

$$\boxtimes_{\gamma Z} = \frac{3\hat{\alpha}_{fZ}}{2\pi} Q_f g_{VA}^{\ell f} \left(\ln \frac{M_Z^2}{m_f^2} + \frac{3}{2} \right), \quad \boxtimes'_{\gamma Z} = \frac{3\hat{\alpha}_{pZ}}{2\pi} Q_f g_{AV}^{\ell f} \left(\ln \frac{M_Z^2}{m_p^2} + \frac{5}{6} \right). \quad (113)$$

The numerical values of these NC couplings are computed using Eqs. (81) and are given in Table 7.

As in Section 4.3 one has to correct for $Q^2 \neq 0$. The only new issue for the g_{AV}^{ef} are the γZ box graphs which still need to be computed for the relevant Q^2 -values and electron beam energies. We expect that in the DIS regime this should be feasible with sufficient accuracy, but we suppose that the numerical answer will not differ very strongly from $\boxtimes_{\gamma Z}$ in Eq. (113). Ignoring this issue, we find for the SLAC [142] and Jefferson Lab DIS experiments, all with Q^2 values around the charm quark threshold,

$$\begin{aligned} g_{AV}^{eq} &\rightarrow g_{AV}^{eq} + 2Q_q \left[\hat{s}_Q^2 - \hat{s}_0^2 + \frac{\alpha}{6\pi} \left(-g_{VA}^{ee} \ln \frac{Q^2}{m_e^2} + \frac{15}{2} - \frac{190}{9} \hat{s}_0^2 + \Delta_Q^{eq} \right) \right] \\ &\approx g_{AV}^{eq} - 0.0011 Q_q \ln \frac{Q^2}{0.14 \text{ GeV}^2}. \end{aligned} \quad (114)$$

The small Q^2 -dependent correction term Δ_Q^{eq} accounts for non-decoupling b quark and τ lepton effects, the non-vanishing masses of the lighter fermions, and some reducible higher-order effects. Similarly,

$$g_{VA}^{eu} \rightarrow g_{VA}^{eu} - 0.0009 \ln \frac{Q^2}{0.078 \text{ GeV}^2}, \quad g_{VA}^{ed} \rightarrow g_{VA}^{ed} + 0.0007 \ln \frac{Q^2}{0.021 \text{ GeV}^2}. \quad (115)$$

The $\boxtimes_{\gamma Z}$ and $\boxtimes'_{\gamma Z}$ contributions induce extra Q^2 -dependences and may change the $A_{LR}^{e\text{DIS}}$ by several ‰.

Ref. [153] obtained $\boxtimes_{\gamma Z}$ for the case of APV, which we represent as a correction relative to Eq. (113),

$$g_{AV}^{eq} \rightarrow g_{AV}^{eq} + \frac{3\hat{\alpha}_{pZ}}{2\pi} Q_q g_{VA}^{eq} \ln \frac{m_p^2}{m_q^2} \approx \begin{cases} g_{AV}^{eu} + 0.00002(4), \\ g_{AV}^{ed} + 0.00002(2), \\ g_{AV}^{ep} + 0.00005(9), \\ g_{AV}^{en} + 0.00006(7), \end{cases} \quad (116)$$

choosing $m_u = 1.07 \text{ GeV}$ and $m_d = 1.14 \text{ GeV}$ to reproduce the result [153] relevant for bound nucleons.

Table 7: SM values of the one-loop and leading two-loop corrected effective NC e couplings for the charged SM fermions and the nucleons.

f	e	u	d	p	n
g_{AV}^{ef}	0.0225	-0.1887	0.3419	-0.0355	0.4950
g_{VA}^{ef}	0.0225	-0.0351	0.0247	-0.0454	0.0144

Likewise, $\boxtimes_{\gamma Z}$ was computed in Ref. [154] for polarized electron scattering at $Q^2 = 0$, resulting in

$$g_{AV}^{ep} \rightarrow g_{AV}^{ep} - 0.0021_{-0.0006}^{+0.0003} \text{ (CEBAF)}, \quad g_{AV}^{ep} \rightarrow g_{AV}^{ep} - 0.0007_{-0.0003}^{+0.0002} \text{ (MESA)}, \quad (117)$$

for $E_e = 1.165$ GeV and $E_e = 200$ MeV, respectively. These shifts are due to the sum of both chirality structures, $\boxtimes_{\gamma Z}$ and $\boxtimes'_{\gamma Z}$, where the latter [155] (which is dominant here but irrelevant for APV) agrees well within the quoted uncertainties with the findings of Refs. [156,157]. The error estimates themselves are currently under discussion, and are expected to improve when more experimental data entering the theoretical dispersion integrals will become available. The effects due to $Q^2 \neq 0$ in the shifts (117) is about -3.5×10^{-5} [157] for Qweak and negligible, and the Q^2 -dependence of the weak mixing angle can be ignored if A_{LR}^{ep} is normalized using the fine structure constant in the Thomson limit (see the footnote to Section 5.1), but the electron charge radius induces the additional shift,

$$g_{AV}^{ep} \rightarrow g_{AV}^{ep} - 0.00008 \ln \frac{Q^2}{0.00021 \text{ GeV}^2}. \quad (118)$$

Finally, the experiment specific adjustments due to $\boxtimes_{\gamma Z}$ and the electron charge radius to be applied to g_{VA}^{ee} for the conditions of the E158 (with a beam energy of about 48 GeV) and MOLLER (11 GeV) experiments are, respectively,

$$g_{VA}^{ee} \rightarrow g_{VA}^{ee} + 0.0010 \pm 0.0004 \text{ (SLC)}, \quad g_{VA}^{ee} \rightarrow g_{VA}^{ee} + 0.0008 \pm 0.0005 \text{ (CEBAF)}. \quad (119)$$

Note, that some contributions have been merged together with other radiative corrections into \mathcal{F}_{QED} [109].

6 Constraints on Supersymmetry

The low energy NC measurements discussed in the previous sections give complementary information on possible physics beyond the SM, especially when compared to Z -pole precision observables as well as direct searches for new particles at high energy colliders. In this section, we illustrate the sensitivity to new physics via a few NC measurements (the weak charges of the electron, the proton and of cesium, NuTeV, and eDIS) using the Minimal Supersymmetric Standard Model (MSSM) as a specific example. For a review of low energy precision tests of supersymmetry, see Ref. [158].

6.1 Minimal Supersymmetric Standard Model

The SM has been very successful in describing the strong, weak and electromagnetic interactions and has been confirmed to high precision by a wide variety of experiments. As reviewed in Section 2.2, the Higgs mechanism is introduced to spontaneously break $SU(2)_L \times U(1)_Y$ down to the electromagnetic gauge group, $U(1)_Q$. Being a fundamental scalar particle, the Higgs boson receives large corrections to

its mass from quantum loop effects, which are quadratic in terms of the cut-off scale Λ_{UV} . If Λ_{UV} is of the order of Planck mass scale, a precise cancellation of 32 orders of magnitude between the tree-level bare Higgs mass squared and the radiative corrections is needed to obtain a physical M_H around the EW scale. If not helped by a symmetry [159], such a high level of fine tuning is referred to as a naturalness problem. Finding a solution to the naturalness problem of the SM Higgs sector (the hierarchy problem) points to physics beyond the SM, such as supersymmetry (SUSY) [160,161], large extra dimensions [162,163], warped extra dimensions [164], little Higgs theories [165,166], composite Higgs models [167], Higgs-less models [168], *etc.*

Supersymmetry is a symmetry under the interchange of bosonic and fermionic degrees of freedom and is considered to be one of the most promising new physics scenarios among various proposals. For each particle in a supersymmetric theory, there exists a superpartner with spin differing by half a unit. *E.g.*, the fermionic superpartners of Higgs bosons are called *Higgsinos*, while the scalar superpartners of quarks and leptons, are called *squarks* and *sleptons*, respectively. The spin-1/2 superpartners of the gauge bosons are called *gluinos*, *winos* and the *bino*. When SUSY is exact, the masses and the gauge quantum numbers of the superpartners are the same, and the couplings are related by the symmetry. These features protect the Higgs mass from receiving the problematic quadratic dependence on Λ_{UV} as these contributions from fermionic and bosonic superpartners cancel. SUSY has to be broken, however, since no scalar-electron with the same mass and coupling of that of the electron has been observed. Soft SUSY breaking by superrenormalizable terms in the Lagrangian, *i.e.*, terms with coefficients of strictly positive mass dimension, is needed to retain the cancellation of the quadratic Λ_{UV} dependence of the Higgs mass corrections.

The remaining logarithmic corrections to M_H are proportional to the soft SUSY breaking masses \tilde{m} ,

$$\Delta M_H^2 \propto -\frac{\tilde{m}^2}{8\pi^2} \ln \frac{\Lambda_{UV}^2}{\tilde{m}^2} + \dots, \quad (120)$$

where \tilde{m} should not exceed a few TeV to avoid reintroduction of the naturalness problem. Besides providing an elegant solution to the hierarchy problem, SUSY offers other attractive features, such as approximate gauge coupling unification, radiatively generated EW symmetry breaking, a dark matter candidate, and (in MSSM extensions) the possibility to generate the baryon asymmetry of the universe.

By definition, the MSSM is the SUSY model with the minimal particle content and provides a useful framework for discussing the phenomenology of low energy SUSY. Note, that the introduction of two Higgs doublets with opposite hypercharge, H_u and H_d , is dictated by the requirement of anomaly cancellation among the Higgsinos, and independently by the holomorphicity of the superpotential. In contrast to the SM, where the same Higgs doublet gives masses to both the up and down type quarks, here they receive their masses from the VEVs of the neutral H_u and H_d , respectively.

The most general MSSM superpotential also includes baryon number (B) and lepton number (L) violating interactions, which lead to rapid proton decay already at the renormalizable level, which is in sharp conflict with bounds on the proton lifetime. One way to eliminate such terms is to introduce a new symmetry called R -parity, defined by conservation of the quantum number,

$$P_R = (-1)^{3(B-L)+2S}, \quad (121)$$

where S is the spin of the particle. All SM particles are assigned $P_R = +1$, while all the superpartners have $P_R = -1$. Exact R -parity has two important phenomenological consequences: (i) The lightest supersymmetric particle (LSP) is absolutely stable. (ii) SM particles are coupled to even numbers of superpartners (usually two). If the LSP is colorless and electrically neutral, it may be a viable candidate to constitute cold dark matter. For low-energy processes involving only SM particles in the initial and final states, such as those of interest in this section, supersymmetric contributions appear only at the loop-level via virtual pair production of superpartners. However, one may relax the constraint of

R -parity conservation while preserving proton stability, *e.g.*, by forbidding only the baryon number violating terms. In this case, the LSP is no longer stable and tree-level SUSY contributions to low energy processes occur through R -parity violating interactions. In what follows, we will consider the implications of both R -parity conserving (RPC) and R -parity violating (RPV) supersymmetry.

The MSSM soft terms contribute masses to the Bino (M_1), Winos (M_2), Gluinos (M_3), the squarks and sleptons, the Higgs bosons, as well as a bilinear Higgs mixing “ B -term”, and trilinear “ A -terms” that couple Higgs scalars with the superpartners of left- and right-handed quarks and leptons. The A -terms and the soft SUSY breaking squark and slepton masses are in general non-diagonal in the flavor basis which could lead to large flavor-changing neutral current (FCNC) effects. They might also have additional phases that cannot be eliminated by field redefinitions, thus inducing new sources of CP-violation. For generic parameter values, the predicted effects are considerably larger than allowed by the experimental limits (the SUSY flavor and CP problems). For illustration, we consider one approach to the flavor problem in which it is assumed that all soft masses of squarks and sleptons are diagonal in the flavor basis and that A -terms are proportional to the corresponding Yukawa matrices. Under these simple assumptions, the mass matrix of the superpartners of the left- and right-handed SM fermions reduces to block-diagonal form of 2×2 sub-matrices for each flavor, governed by mixing angles $\theta_{\tilde{f}}$.

After EW symmetry breaking, the neutral gauginos and Higgsinos, \tilde{B} , \tilde{W}^0 , \tilde{H}_d^0 , \tilde{H}_u^0 , mix with each other. The mass eigenstates are called neutralinos, χ_i^0 ($i = 1 \cdots 4$), with $m_{\chi_1^0} < m_{\chi_2^0} < m_{\chi_3^0} < m_{\chi_4^0}$ by definition. In the limit, $M_Z \ll M_1, M_2, |\mu|$, each χ_i^0 is a pure gaugino or Higgsino state, but in general the χ_i^0 are mixtures. Similarly, charged gauginos and Higgsinos, \tilde{W}^+ , \tilde{H}_u^+ , \tilde{W}^- , \tilde{H}_d^- , mix to form chargino states, χ_i^\pm ($i = 1, 2$), with $m_{\chi_1^\pm} < m_{\chi_2^\pm}$. The $SU(3)_C$ gluinos are color octet fermions, and cannot mix with other particles in the MSSM. In phenomenological studies one usually assumes the mass unification relation at the EW scale $M_3 : M_2 : M_1 = \alpha_3 : \alpha_2 : \alpha_1 \approx 7 : 2 : 1$. However, such a relation need not hold in general and M_3 , M_2 and M_1 could be completely independent of each other.

The gauge interactions involving superpartners in the MSSM can be obtained from the usual SM gauge interactions by replacing two of the SM particles with their superpartners. Similarly, Higgs-squark-squark and Higgsino-quark-squark couplings can be obtained through Yukawa interactions, which also give rise to additional Higgs-Higgs-squark-squark couplings. The A -terms give rise to additional Higgs-squark-squark couplings. Analogous remarks apply to the leptonic sector.

6.2 R -parity conserving MSSM contributions to neutral current processes

The precise measurements of the electron and proton weak charges could probe both the supersymmetric loop effects as well as the tree-level RPV contributions. For RPC SUSY, contributions to Q_W^e and Q_W^p , or equivalently to g_{AV}^{ee} and g_{AV}^{ep} , appear at the loop-level and have been analyzed in detail in Ref. [169]. The results are summarized and updated in Figure 10, taking into account the latest limits from superparticle searches at the LHC [170,171], as well as tighter constraints on the oblique parameters [15]. We plotted the contributions to g_{AV}^{ep} *vs.* those to g_{AV}^{ee} , normalized to the respective SM values. The dots show the results of a random scan over a range of MSSM parameters. The loop corrections in the RPC case are nearly always positive and can reach 2–3% for g_{AV}^{ep} . For g_{AV}^{ee} it can be even larger but this is not supported by the result of E158 [59] which observed a suppressed value compared to the SM. The planned PVES experiments [112,139] would reach factors of five and two better than E158 and Qweak, respectively, and would provide very significant constraints on the loop effects in RPC SUSY.

The corrections to $g_{AV}^{ee,ep}$ are dominated by the SUSY contribution proportional to \hat{s}_Z^2 , which is identical for ee and ep scattering. Such dominance produces a nearly linear correlation between these two couplings. This universal correction is almost always negative, predicting an apparent reduction in the extracted value of \hat{s}_Z^2 from PVES experiments.

The possible effects of new physics on the $Q_W^{Z,N}$, or equivalently, $Zg_{AV}^{ep} + Ng_{AV}^{en}$, can be written as a sum of the corresponding effects on $g_{AV}^{eu,ed}$. Since the sign of $\delta g_{AV}^f/g_{AV}^f$ due to superpartner loops is

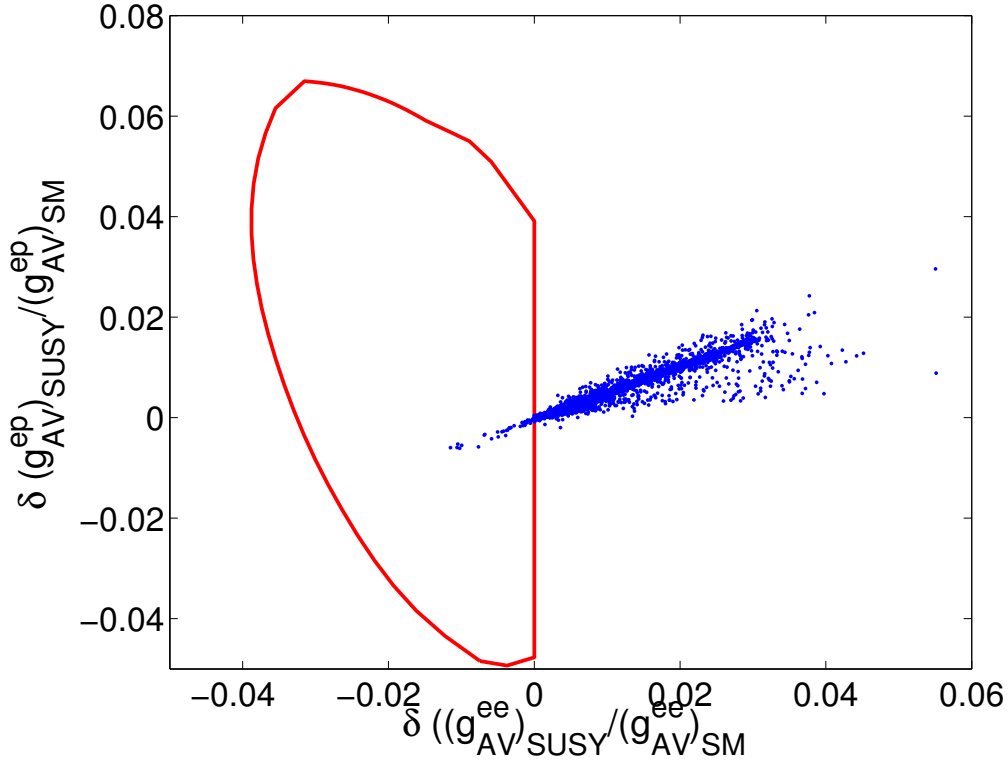


Figure 10: Relative shifts in g_{AV}^{ee} and g_{AV}^{ep} (normalized to the respective SM values) due to SUSY effects. The dots indicate the RPC corrections for ~ 3000 randomly generated SUSY-breaking parameters. The interior of the truncated elliptical region gives the possible shifts due to the RPV SUSY interactions at the 95% CL. (Figure updated from Ref. [169].)

nearly always the same, and since $g_{AV}^{eu} < 0$ and $g_{AV}^{ed} > 0$ in the SM, a strong cancellation between δg_{AV}^{eu} and δg_{AV}^{ed} occurs in heavy nuclei. This means that the magnitude of superpartner loop contributions to the weak charge of cesium, Q_W^{Cs} , is generally less than about 0.2%, and is equally likely to have either sign. Since the total uncertainty is presently about 0.6% [122], it does not substantially constrain the RPC SUSY parameter space. This contrasts with a class of models with extra Z bosons, where sizable shifts in $g_{AV}^{ee,ep}$ would also imply observable deviations in Q_W^{Cs} [111]. In the case where such models and the MSSM have similar effects on g_{AV}^{ee} and g_{AV}^{ep} , the determination of Q_W^{Cs} may tell these two apart.

In addition to the g_{AV}^{eq} (C_{1q}), the RPC version of the MSSM also affects the g_{VA}^{eq} (C_{2q}) which can be probed in eDIS [143,144] as discussed in Section 5.3. The shifts in A_{LR}^{eDIS} are correlated with those in g_{AV}^{ee} and g_{AV}^{ep} and may reach 0.7% [173].

The RPC contributions to R_ν and $R_{\bar{\nu}}$ are highly correlated and can reach 1.5×10^{-3} [172,174]. Their sign is almost always positive, which is in conflict with the sign of the NuTeV anomaly. Contributions from gluino loop with nearly degenerate first generation up-type squark and down-type squarks and close to maximal left-right mixing could admit a negative loop contribution. However, this corner of parameter space is disfavored theoretically and has tensions with other precision electroweak inputs. In any case, these negative gluino contributions are too small to fully account for NuTeV.

6.3 R -parity violating supersymmetry

Additional B - and L -violating interactions may appear in the MSSM if RPV is allowed. Rapid proton decay can still be avoided if we only turn on B or L violating terms, but not both simultaneously. For

low energy processes where light quarks are present in the initial and final states, the RPV terms that are of interest are the Yukawa-type interactions,

$$\mathcal{L}_{\text{RPV}}^{\Delta L=1} = \lambda_{ijk} \left(\frac{1}{2} L_i L_j \tilde{e}_k^\dagger + \tilde{L}_i L_j \tilde{e}_k^\dagger \right) + \lambda'_{ijk} (L_i Q_j \tilde{d}_k^\dagger + \tilde{L}_i Q_j \tilde{d}_k^\dagger + L_i \tilde{Q}_j \tilde{d}_k^\dagger), \quad (122)$$

$$\mathcal{L}_{\text{RPV}}^{\Delta B=1} = \lambda''_{ijk} (\bar{u}_i^\dagger \bar{d}_j \tilde{d}_k^\dagger + \tilde{u}_i^\dagger \bar{d}_j \tilde{d}_k^\dagger), \quad (123)$$

which will contribute via the exchange of heavy squarks or sleptons. For small momentum transfers, $q^2 \ll m_{\tilde{f}}^2$, the corrections can be parametrized in terms of

$$\Delta_{ijk}(\tilde{f}) \equiv \frac{|\lambda_{ijk}|^2}{4} \frac{v^2}{m_{\tilde{f}}^2} \geq 0, \quad (124)$$

and similarly for the primed and doubly primed quantities. The shifts in the couplings are then [175],

$$\delta g_{AV}^{ee} \approx -[g_{AV}^{ee} + 2\lambda_x] \Delta_{12k}(\tilde{e}_R^k), \quad (125)$$

$$\delta g_{AV}^{ep} \approx -[g_{AV}^{ep} - 2\lambda_x] \Delta_{12k}(\tilde{e}_R^k) - 2\Delta'_{11k}(\tilde{d}_R^k) + \Delta'_{1k1}(\tilde{q}_L^k), \quad (126)$$

$$\delta g_{AV}^{eu} = -\left[g_{AV}^{eu} - \frac{4}{3}\lambda_x\right] \Delta_{12k}(\tilde{e}_R^k) - \Delta'_{11k}(\tilde{d}_R^k), \quad \delta g_{AV}^{ed} = -\left[g_{AV}^{ed} + \frac{2}{3}\lambda_x\right] \Delta_{12k}(\tilde{e}_R^k) + \Delta'_{1k1}(\tilde{q}_L^k), \quad (127)$$

$$\delta g_{VA}^{eu} = -[g_{VA}^{eu} - 2\lambda_x] \Delta_{12k}(\tilde{e}_R^k) - \Delta'_{11k}(\tilde{d}_R^k), \quad \delta g_{VA}^{ed} = -[g_{VA}^{ed} + 2\lambda_x] \Delta_{12k}(\tilde{e}_R^k) - \Delta'_{1k1}(\tilde{q}_L^k), \quad (128)$$

where,

$$\lambda_x = \frac{\hat{s}_Z^2 \hat{c}_Z^2}{1 - 2\hat{s}^2} \frac{1}{1 - \Delta \hat{r}_Z^{\text{SM}}}. \quad (129)$$

Since the $\Delta_{ijk}^{(\prime)}$ are non-negative, Eq. (125) shows that the shifts in the g_{AV}^{ee} are negative semidefinite, while according to Eq. (126) those in the g_{AV}^{ep} can have either sign depending on the relative magnitudes of Δ_{12k} , Δ'_{11k} , and Δ'_{1k1} .

Quantities such as the Δ_{ijk} are also constrained by other precision measurements and rare decays. A summary of the current experimental bounds is shown in Table 8. It includes CKM unitarity tests obtained from superallowed nuclear β -decays (constraining $|V_{ud}|$ [176]) and the kaon-decay determination of V_{us} , the APV measurement of Q_W^{Cs} [122,125], the ratio $R_{e/\mu}$ [177,178] of π_{l2} decays [179,180], and the allowed range for $\Delta \hat{r}$ defined in Eq. (48)]. We also indicate the sensitivity to the various $\Delta_{ijk}^{(\prime)}(\tilde{f})$.

The 95% CL allowed region in the $\delta g_{AV}^{ep}/g_{AV}^{ep}$ vs. $\delta g_{AV}^{ee}/g_{AV}^{ee}$ plane is shown by the closed curve in Figure 10. Note, that the truncation of the initially elliptical curve is due to the inequality in Eq. (124). The corrections to g_{AV}^{ee} from RPV SUSY are always negative and less than about 4% in magnitude, while those to g_{AV}^{ep} vary in the range of -5% to 7% . In addition, the prospective effects of RPV SUSY where $\delta g_{AV}^{ep}/g_{AV}^{ep}$ can have either sign, are quite distinct from SUSY loops where it is non-negative. Thus, a comparison of the results for the two PVES experiments could help determine whether this extension of the MSSM is favored over other new physics scenarios (see also Ref. [111]).

Given the 95% CL region for the RPV coefficients, the maximum RPV correction to A_{LR}^{eDIS} is about $\pm 0.4\%$, close to the precision proposed in Ref. [144]. The RPV effects would induce opposite shifts in A_{LR}^{eDIS} and g_{AV}^{ee} , whereas the loop corrections are positive in both cases. A sizable positive shift in g_{AV}^{ep} due to the RPV contributions could correspond to a tiny effect in A_{LR}^{eDIS} . The addition of an eDIS measurement would provide a useful complement to the PVES ee and ep measurements, assuming it can be performed with $\sim 0.4\%$ precision or better.

Similarly, the shifts in $R_{\nu(\bar{\nu})}$ introduced by the tree-level RPV interactions are given by,

$$\delta R_{\nu(\bar{\nu})} = \frac{1+r}{r} \left[-\frac{4}{3} g_{LL}^{\nu u} + \frac{2}{3} g_{LL}^{\nu d} \right] \lambda_x \Delta_{12k}(\tilde{e}_R^k) - 2 [R_{\nu(\bar{\nu})}^{\text{SM}} + g_{LL}^{\nu d}] \Delta'_{21k}(\tilde{d}_R^k) + \frac{2}{r} g_{LR}^{\nu d} \Delta'_{2k1}(\tilde{d}_L^k). \quad (130)$$

Table 8: RPV contributions to $|V_{ud}|^2$, Q_W^{Cs} , $R_{e/\mu}$ and $\Delta\hat{r}$. $\delta|V_{ud}|^2/|V_{ud}|^2$ are the corrections to $|V_{ud}|^2$ extracted from beta-decay that are allowed by first row CKM unitarity tests. The mid columns display the coefficients of the various corrections from Δ'_{ijk} and Δ_{12k} . The last column gives the values extracted from experiment assuming only SM contributions.

Quantity	$\Delta'_{11k}(\tilde{d}_R^k)$	$\Delta'_{1k1}(\tilde{q}_L^k)$	$\Delta_{12k}(\tilde{e}_R^k)$	$\Delta'_{21k}(\tilde{d}_R^k)$	Value
$\delta V_{ud} ^2/ V_{ud} ^2$	2	0	-2	0	-0.0001 ± 0.0006
$\delta Q_W^{Cs}/Q_W^{Cs}$	-4.82	5.41	0.05	0	-0.0089 ± 0.0059
$\delta R_{e/\mu}$	2	0	0	-2	-0.0034 ± 0.0030
$\Delta\hat{r}$	0	0	1	0	-0.00002 ± 0.00045

While $\Delta_{12k}(\tilde{e}_R^k)$ and $\Delta'_{21k}(\tilde{d}_R^k)$ are constrained by other precision EW data, $\Delta'_{2k1}(\tilde{d}_L^k)$ is relatively unconstrained. The present constraints on $\Delta_{12k}(\tilde{e}_R^k)$ from other EW observables, as listed in Table 8, however, are fairly stringent. The possible effects on R_ν and $R_{\bar{\nu}}$ from RPV interactions are by and large positive. Negative corrections are also possible, but they are too small to be interesting [172].

We have used SUSY as an example of how new physics may affect the low energy NC precision observables. In addition, there are various studies in the literature exploring other types of new physics, such as models with extra Z' bosons [181–187] and leptoquarks [133,188]. The bottom line is that the combination of various NC experiments can distinguish between different new physics scenarios, as illustrated in Refs. [169,181,183,185]. *E.g.*, while both the superpartner loops and leptoquark exchange give positive contributions to the proton weak charge, only the MSSM gives rise to a sizable effect on the electron weak charge [111,133]. For the class of Z' theories based on the E_6 gauge group with Z' masses $\lesssim 1$ TeV, the effects on Q_W^p and Q_W^e also correlate, but $\delta Q_W^{e,p}/Q_W^{e,p}$ can have either sign [111,133]. Finally, in the case where E_6 Z' models and the MSSM have similar effects on g_{AV}^{ep} and g_{AV}^{ee} , the determination of Q_W^{Cs} can further tell these two apart.

7 Conclusions

In this review, we surveyed low energy neutral current measurements, including neutrino scattering, parity-violating electron scattering, and atomic parity violation. We reviewed the experimental status and the theoretical challenges of these observables, and pointed to future experiments that are either planned or proposed. We also explored the sensitivity of those measurement to new physics, using the minimal supersymmetric Standard Model as a specific example. Furthermore, we illustrated how the interplay between the various NC observables provides extra discriminating power between different types of physics beyond the SM.

While the direct measurements of W and Z properties have reached per mille precision, and the LHC at its design energy of 14 TeV could produce strong interacting particles with masses in the few TeV range, the low energy precision measurements provide an alternative probe of new physics. *E.g.*, they are sensitive to new physics that does not mix with W and Z bosons. With the high statistics achieved at the intensity frontier and the advances in both the theoretical and experimental sides, they serve as indispensable complements to the energy frontier. If a significant deviation from the SM prediction is observed in a low energy neutral current observable, comparison with other precision measurements and the collider results will sharpen our understanding of physics beyond the SM.

Acknowledgements

It is a pleasure to thank Krishna Kumar and Paul Langacker for a careful reading of the manuscript and stimulating discussions. The work of J.E. was supported by CONACyT (México) projects 82291–F and 15 1234 and by PAPIIT (DGAPA–UNAM) project IN106913. The work of S.S. was supported by the Department of Energy under Grant DE–FG02–04ER–41298.

References

- [1] J. L. Hewett *et al.*, arXiv:1205.2671 [hep-ex]
- [2] J. Erler and M. J. Ramsey-Musolf, *Prog. Part. Nucl. Phys.* 54 (2005) 351
- [3] K. S. Kumar, S. Mantry, W. J. Marciano and P. A. Souder, arXiv:1302.6263 [hep-ex]
- [4] P. Langacker, *The Standard Model and Beyond* (Taylor & Francis, Boca Raton, FL, 2010)
- [5] S. Weinberg, *Phys. Rev.* 138 (1965) B988
- [6] S. Weinberg, *Phys. Rev. Lett.* 19 (1967) 1264
- [7] S. L. Glashow, *Nucl. Phys.* 22 (1961) 579
- [8] For a review, see A. Djouadi, *Phys. Rep.* 457 (2008) 1
- [9] P. W. Higgs, *Phys. Lett.* 12 (1964) 132 and *Phys. Rev. Lett.* 13 (1964) 508
- [10] G. S. Guralnik, C. R. Hagen and T. W. B. Kibble, *Phys. Rev. Lett.* 13 (1964) 585
- [11] F. Englert and R. Brout, *Phys. Rev. Lett.* 13 (1964) 321
- [12] T. W. B. Kibble, *Phys. Rev.* 155 (1967) 1554
- [13] J. Goldstone, *Nuovo Cim.* 19 (1961) 154
- [14] D. M. Webber *et al.* (MuLan Collaboration), *Phys. Rev. Lett.* 106 (2011) 041803 and *ibid.* 079901
- [15] J. Erler and P. Langacker, *Electroweak Model and Constraints on New Physics*, pp. 136–156 of Ref. [16]
- [16] J. Beringer *et al.* (Particle Data Group), *Phys. Rev. D* 86 (2012) 010001
- [17] J. Erler and M. J. Ramsey-Musolf, *Phys. Rev. D* 72 (2005) 073003
- [18] A. Czarnecki and W. J. Marciano, *Int. J. Mod. Phys. A* 15 (2000) 2365
- [19] S. Weinberg, *Phys. Rev. Lett.* 43 (1979) 1566
- [20] K. Abe *et al.* (SLD Collaboration), *Phys. Rev. Lett.* 84 (2000) 5945
- [21] The ALEPH, DELPHI, L3, OPAL and SLD Collaborations, the LEP Electroweak Working Group and the SLD Electroweak and Heavy Flavour Groups, *Phys. Rep.* 427 (2006) 257
- [22] K. Abe *et al.* (SLD Collaboration), *Phys. Rev. Lett.* 85 (2000) 5059
- [23] K. Abe *et al.* (SLD Collaboration), *Phys. Rev. Lett.* 86 (2001) 1162
- [24] K. Abe *et al.* (SLD Collaboration), *Phys. Rev. Lett.* 78 (1997) 17
- [25] P. Abreu *et al.* (DELPHI Collaboration), *Z. Phys. C* 67 (1995) 1
- [26] V. M. Abazov *et al.* (DØ Collaboration), *Phys. Rev. D* 84 (2011) 012007
- [27] J. Han (CDF Collaboration), in the Proceedings of DPF–2011, arXiv:1110.0153 [hep-ex]
- [28] S. Chatrchyan *et al.* (CMS Collaboration), *Phys. Rev. D* 84 (2011) 112002
- [29] W. Hollik, *Predictions for e^+e^- processes*, pp. 117–169 of Ref. [30]
- [30] P. Langacker (ed.), *Precision tests of the standard electroweak model*, Advanced series on directions in high energy physics: 14 (World Scientific, Singapore, Singapore, 1995)

- [31] A. Freitas and Y. C. Huang, *JHEP* 1208 (2012) 050
- [32] J. Alcaraz *et al.* (ALEPH, DELPHI, L3 and OPAL Collaborations and LEP Electroweak Working Group), arXiv:hep-ex/0612034
- [33] Tevatron Electroweak Working Group (CDF and DØ Collaborations), arXiv:1204.0042 [hep-ex]
- [34] M. Beneke, P. Falgari, C. Schwinn, A. Signer and G. Zanderighi, *Nucl. Phys. B* 792 (2008) 89
- [35] G. Zanderighi, <http://www.ggi.fi.infn.it/talks/talk484.pdf>
- [36] T. Aaltonen *et al.* (CDF Collaboration), *Phys. Rev. Lett.* 108 (2012) 151803
- [37] Y. Zeng, http://www.phy.duke.edu/~yz38/wmw_meeting/CollabMeeting_Wmass_2012Mar29.pdf
- [38] A. Sirlin, *Phys. Rev. D* 22 (1980) 971
- [39] G. Degrossi, S. Fanchiotti and A. Sirlin, *Nucl. Phys. B* 351 (1991) 49
- [40] J. Erler, *Phys. Rev. D* 59 (1999) 054008
- [41] M. Davier, A. Hoecker, B. Malaescu and Z. Zhang, *Eur. Phys. J. C* 71 (2011) 1515
- [42] Tevatron Electroweak Working Group and CDF and DØ Collaborations, arXiv:1107.5255 [hep-ex]
- [43] ATLAS and CMS Collaborations, <https://twiki.cern.ch/twiki/bin/view/CMSPublic/PhysicsResultsTOP12001>
- [44] K. G. Chetyrkin and M. Steinhauser, *Nucl. Phys. B* 573 (2000) 617
- [45] J. Erler, in the Proceedings of the Physics at Run II Workshop at FNAL, arXiv:hep-ph/0005084
- [46] M. Beneke, *Phys. Rep.* 317 (1999) 1
- [47] G. Aad *et al.* (ATLAS Collaboration), arXiv:1207.0319 [hep-ex].
- [48] CMS Collaboration, <http://cdsweb.cern.ch/record/1429928/files/HIG-12-008-pas.pdf>
- [49] J. Erler, arXiv:1201.0695 [hep-ph]
- [50] R. Barate *et al.* (LEP Working Group for Higgs Boson Searches and ALEPH, DELPHI, L3 and OPAL Collaborations), *Phys. Lett. B* 565 (2003) 61
- [51] Tevatron New-Phenomena and Higgs Working Group and CDF and DØ Collaborations, arXiv:1203.3774 [hep-ex]
- [52] W. J. Marciano and J. L. Rosner, *Phys. Rev. Lett.* 65 (1990) 2963
- [53] D. C. Kennedy and P. Langacker, *Phys. Rev. Lett.* 65 (1990) 2967
- [54] G. Altarelli, R. Barbieri and S. Jadach, *Nucl. Phys. B* 369 (1992) 3
- [55] M. E. Peskin and T. Takeuchi, *Phys. Rev. D* 46 (1992) 381
- [56] M. J. G. Veltman, *Nucl. Phys. B* 123 (1977) 89
- [57] I. Maksymyk, C. P. Burgess and D. London, *Phys. Rev. D* 50 (1994) 529
- [58] H. Davoudiasl, H. S. Lee and W. J. Marciano, *Phys. Rev. D* 85 (2012) 115019
- [59] P. L. Anthony *et al.* (SLAC E158 Collaboration), *Phys. Rev. Lett.* 95 (2005) 081601
- [60] R. D. Young, R. D. Carlini, A. W. Thomas and J. Roche, *Phys. Rev. Lett.* 99 (2007) 122003
- [61] C. Albright *et al.*, arXiv:hep-ex/0008064
- [62] J. Panman, *Neutrino-electron scattering*, pp. 504–544 of Ref. [30]
- [63] F. J. Hasert *et al.* (Gargamelle Collaboration), *Phys. Lett. B* 46 (1973) 121
- [64] S. Sarantakos, A. Sirlin and W. J. Marciano, *Nucl. Phys. B* 217 (1983) 84
- [65] J. Dorenbosch *et al.* (CHARM Collaboration), *Z. Phys. C* 41 (1989) 567
- [66] P. Vilain *et al.* (CHARM II Collaboration), *Phys. Lett. B* 335 (1994) 246
- [67] L. A. Ahrens *et al.* (CALO Collaboration), *Phys. Rev. D* 41 (1990) 3297
- [68] R. C. Allen *et al.* (CNTR Collaboration), *Phys. Rev. D* 47 (1993) 11

- [69] L. B. Auerbach *et al.* (LSND Collaboration), *Phys. Rev. D* 63 (2001) 112001
- [70] M. Deniz *et al.* (TEXONO Collaboration), *Phys. Rev. D* 81 (2010) 072001
- [71] F. Perrier, *The Measurement of electroweak parameters from deep inelastic neutrino scattering*, pp. 385–490 of Ref. [30]
- [72] J. M. Conrad, M. H. Shaevitz and T. Bolton, *Rev. Mod. Phys.* 70 (1998) 1341
- [73] C. H. Llewellyn Smith, *Nucl. Phys. B* 228 (1983) 205
- [74] E. A. Paschos and L. Wolfenstein, *Phys. Rev. D* 7 (1973) 91
- [75] B. A. Dobrescu and R. K. Ellis, *Phys. Rev. D* 69 (2004) 114014
- [76] C. G. Callan, Jr. and D. J. Gross, *Phys. Rev. Lett.* 22 (1969) 156
- [77] M. Glück, P. Jimenez-Delgado and E. Reya, *Phys. Rev. Lett.* 95 (2005) 022002
- [78] J. T. Londergan and A. W. Thomas, *Phys. Rev. D* 67 (2003) 111901
- [79] I. C. Cloët, W. Bentz and A. W. Thomas, *Phys. Rev. Lett.* 102 (2009) 252301
- [80] K. P. O. Diener, S. Dittmaier and W. Hollik, *Phys. Rev. D* 69 (2004) 073005
- [81] A. B. Arbuzov, D. Y. Bardin and L. V. Kalinovskaya, *JHEP* 0506 (2005) 078
- [82] J. V. Allaby *et al.* (CHARM Collaboration), *Z. Phys. C* 36 (1987) 611
- [83] A. Blondel *et al.* (CDHS Collaboration), *Z. Phys. C* 45 (1990) 361
- [84] K. S. McFarland *et al.* (CCFR Collaborations), *Eur. Phys. J. C* 1 (1998) 509
- [85] G. P. Zeller *et al.* (NuTeV Collaboration), *Phys. Rev. Lett.* 88 (2002) 091802
- [86] U. Amaldi *et al.*, *Phys. Rev. D* 36 (1987) 1385
- [87] A. K. Mann, *Neutrino proton elastic scattering*, pp. 491–503 of Ref. [30]
- [88] D. B. Leinweber *et al.*, *Phys. Rev. Lett.* 94 (2005) 212001
- [89] D. B. Leinweber *et al.*, *Phys. Rev. Lett.* 97 (2006) 022001
- [90] Z. Ahmed *et al.* (HAPPEX Collaboration), *Phys. Rev. Lett.* 108 (2012) 102001
- [91] S. Baunack *et al.* (PVA4 Collaboration), *Phys. Rev. Lett.* 102 (2009) 151803
- [92] D. Androić *et al.* (GØ Collaboration), *Phys. Rev. Lett.* 104 (2010) 012001
- [93] R. Gonzalez-Jimenez, J. A. Caballero and T. W. Donnelly, arXiv:1111.6918 [nucl-th]
- [94] D. S. Armstrong and R. D. McKeown, *Ann. Rev. Nucl. Part. Sci.* 62 (2012) 337
- [95] S. Weinberg, *Phys. Rev.* 112 (1958) 1375
- [96] J. Horstkotte *et al.* (BNL–E–613 Collaboration), *Phys. Rev. D* 25 (1982) 2743
- [97] L. A. Ahrens *et al.* (BNL–E–734 Collaboration), *Phys. Rev. Lett.* 35 (1975) 785
- [98] P. Zucchelli, *Phys. Lett. B* 532 (2002) 166
- [99] V. Antonelli, G. Battistoni, P. Ferrario and S. Forte, *Nucl. Phys. Proc. Suppl.* 168 (2007) 192
- [100] C. T. Kullenberg *et al.* (NOMAD Collaboration), *Phys. Lett. B* 682 (2009) 177
- [101] Q. Wu *et al.* (NOMAD Collaboration), *Phys. Lett. B* 660 (2008) 19
- [102] D. Rein and L. M. Sehgal, *Nucl. Phys. B* 223 (1983) 29
- [103] H. J. Grabosch *et al.* (SKAT Collaboration), *Z. Phys. C* 31 (1986) 203
- [104] F. Bergsma *et al.* (CHARM Collaboration), *Phys. Lett. B* 157 (1985) 469
- [105] P. Vilain *et al.* (CHARM II Collaboration), *Phys. Lett. B* 313 (1993) 267
- [106] W. J. Marciano and A. Sirlin, *Phys. Rev. D* 22 (1980) 2695
- [107] E. Derman and W. J. Marciano, *Annals Phys.* 121 (1979) 147
- [108] V. A. Zykunov, *Phys. Atom. Nucl.* 67 (2004) 1342

- [109] V. A. Zykunov, J. Suarez, B. A. Tweedie and Y. G. Kolomensky, arXiv:hep-ph/0507287
- [110] A. Czarnecki and W. J. Marciano, *Phys. Rev. D* 53 (1996) 1066
- [111] J. Erler, A. Kurylov and M. J. Ramsey-Musolf, *Phys. Rev. D* 68 (2003) 016006
- [112] J. Mammei *et al.* (MOLLER Collaboration), *Nuovo Cim. C* 035N04 (2012) 203
- [113] M. A. Bouchiat and L. Pottier, *Science* 234 (1986) 1203
- [114] B. P. Masterson and C. E. Wieman, *Atomic parity nonconservation experiments*, pp. 545–576 of Ref. [30]
- [115] C. S. Wood *et al.*, *Science* 275 (1997) 1759
- [116] J. Guéna, M. Lintz and M. A. Bouchiat, arXiv:physics/0412017
- [117] N. H. Edwards, S. J. Phipp, P. E. G. Baird and S. Nakayama, *Phys. Rev. Lett.* 74 (1995) 2654
- [118] P. A. Vetter *et al.*, *Phys. Rev. Lett.* 74 (1995) 2658
- [119] S. A. Blundell, W. R. Johnson and J. R. Sapirstein, *The Theory of atomic parity violation*, pp. 577–598 of Ref. [30]
- [120] J. S. M. Ginges and V. V. Flambaum, *Phys. Rep.* 397 (2004) 63
- [121] S. G. Porsev, K. Beloy and A. Derevianko, *Phys. Rev. Lett.* 102 (2009) 181601
- [122] V. A. Dzuba, J. C. Berengut, V. V. Flambaum and B. Roberts, arXiv:1207.5864 [hep-ph]
- [123] Ya. B. Zeldovich, *Sov. Phys. JETP* 6 (1958) 1184
- [124] W. C. Haxton and C. E. Wieman, *Ann. Rev. Nucl. Part. Sci.* 51 (2001) 261
- [125] S. C. Bennett and C. E. Wieman, *Phys. Rev. Lett.* 82 (1999) 2484
- [126] M. A. Bouchiat and J. Guéna, *J. Phys. France* 49 (1988) 2037
- [127] V. A. Dzuba, V. V. Flambaum, P. G. Silvestrov and O. P. Sushkov, *J. Phys. B* 20 (1987) 3297
- [128] J. L. Rosner, *Phys. Rev. D* 53 (1996) 2724
- [129] S. J. Pollock, E. N. Fortson and L. Wilets, *Phys. Rev. C* 46 (1992) 2587
- [130] B. Q. Chen and P. Vogel, *Phys. Rev. C* 48 (1993) 1392
- [131] B. A. Brown, A. Derevianko and V. V. Flambaum, *Phys. Rev. C* 79 (2009) 035501
- [132] S. Abrahamyan *et al.* (PREX Collaboration), *Phys. Rev. Lett.* 108 (2012) 112502
- [133] M. J. Ramsey-Musolf, *Phys. Rev. C* 60 (1999) 015501
- [134] R. W. Dunford and R. J. Holt, *J. Phys. G* 34 (2007) 2099
- [135] J. A. Behr and G. Gwinner, *J. Phys. G* 36 (2009) 033101
- [136] L. W. Wansbeek *et al.*, *Phys. Rev. A* 78 (2008) 050501(R)
- [137] D. S. Armstrong *et al.* (Qweak Collaboration), arXiv:1202.1255 [physics.ins-det]
- [138] M. Gorchtein and C. J. Horowitz, *Phys. Rev. Lett.* 102 (2009) 091806
- [139] D. Becker, S. Baunack, and F. E. Maas, *Hyperfine Interact.* 214 (2013) 141
- [140] P. A. Souder *et al.*, *Phys. Rev. Lett.* 65 (1990) 694
- [141] P. A. Souder, *Charged lepton hadron asymmetries in fixed target experiments*, pp. 599–625 of Ref. [30]
- [142] C. Y. Prescott *et al.*, *Phys. Lett. B* 84 (1979) 524
- [143] X. Zheng *et al.* (Jefferson Lab Hall A Collaboration), *Nuovo Cim. C* 035N04 (2012) 72
- [144] P. A. Souder (SOLID Collaboration), *AIP Conf. Proc.* 1441 (2012) 123
- [145] A. Argento *et al.*, *Phys. Lett. B* 120 (1983) 245
- [146] S. L. Zhu, S. J. Puglia, B. R. Holstein and M. J. Ramsey-Musolf, *Phys. Rev. D* 62 (2000) 033008

- [147] D. T. Spayde *et al.* (SAMPLE Collaboration), *Phys. Rev. Lett.* 84 (2000) 1106
- [148] R. Hasty *et al.* (SAMPLE Collaboration), *Science* 290 (2000) 2117
- [149] W. Heil *et al.*, *Nucl. Phys. B* 327 (1989) 1
- [150] W. J. Marciano and A. Sirlin, *Phys. Rev. D* 27 (1983) 552
- [151] W. J. Marciano, *Radiative corrections to neutral current processes*, pp. 170–200 of Ref. [30]
- [152] W. J. Marciano and A. Sirlin, *Phys. Rev. D* 29 (1984) 75
- [153] P. G. Blunden, W. Melnitchouk and A. W. Thomas, *Phys. Rev. Lett.* 109 (2012) 262301
- [154] P. G. Blunden, W. Melnitchouk and A. W. Thomas, *Phys. Rev. Lett.* 107 (2011) 081801
- [155] A. Sibirtsev, P. G. Blunden, W. Melnitchouk and A. W. Thomas, *Phys. Rev. D* 82 (2010) 013011
- [156] B. C. Rislow and C. E. Carlson, *Phys. Rev. D* 83 (2011) 113007
- [157] M. Gorchtein, C. J. Horowitz and M. J. Ramsey-Musolf, *Phys. Rev. C* 84 (2011) 015502
- [158] M. J. Ramsey-Musolf and S. Su, *Phys. Rep.* 456 (2008) 1
- [159] G. 't Hooft, *NATO Adv. Study Inst. Ser. B Phys.* 59 (1980) 135
- [160] H. E. Haber and G. L. Kane, *Phys. Rep.* 117 (1985) 75
- [161] S. P. Martin, arXiv:hep-ph/9709356
- [162] N. Arkani-Hamed, S. Dimopoulos and G. R. Dvali, *Phys. Lett. B* 429 (1998) 263
- [163] I. Antoniadis, N. Arkani-Hamed, S. Dimopoulos and G. R. Dvali, *Phys. Lett. B* 436 (1998) 257
- [164] L. Randall and R. Sundrum, *Phys. Rev. Lett.* 83 (1999) 4690 and *ibid.* 83 (1999) 3370
- [165] N. Arkani-Hamed, A. G. Cohen and H. Georgi, *Phys. Lett. B* 513 (2001) 232
- [166] N. Arkani-Hamed *et al.*, *JHEP* 0208 (2002) 021
- [167] R. Harnik, G. D. Kribs, D. T. Larson and H. Murayama, *Phys. Rev. D* 70 (2004) 015002
- [168] C. Csaki, C. Grojean, L. Pilo and J. Terning, *Phys. Rev. Lett.* 92 (2004) 101802
- [169] A. Kurylov, M. J. Ramsey-Musolf and S. Su, *Phys. Rev. D* 68 (2003) 035008
- [170] G. Aad *et al.* (ATLAS Collaboration), *Phys. Lett. B* 718 (2013) 879
- [171] S. Chatrchyan *et al.* (CMS Collaboration), arXiv:1303.2985 [hep-ex]
- [172] A. Kurylov, M. J. Ramsey-Musolf and S. Su, *Nucl. Phys. B* 667 (2003) 321
- [173] A. Kurylov, M. J. Ramsey-Musolf and S. Su, *Phys. Lett. B* 582 (2004) 222
- [174] S. Davidson, S. Forte, P. Gambino, N. Rius and A. Strumia, *JHEP* 0202 (2002) 037
- [175] M. J. Ramsey-Musolf, *Phys. Rev. D* 62 (2000) 056009
- [176] J. C. Hardy and I. S. Towner, *Phys. Rev. C* 79 (2009) 055502
- [177] D. I. Britton *et al.*, *Phys. Rev. Lett.* 68 (1992) 3000
- [178] G. Czapek *et al.*, *Phys. Rev. Lett.* 70 (1993) 17
- [179] V. Cirigliano and I. Rosell, *JHEP* 0710 (2007) 005
- [180] S. Bauman, J. Erler and M. J. Ramsey-Musolf, *Phys. Rev. D* 87 (2013) 035012
- [181] W. F. Chang, J. N. Ng and J. M. S. Wu, *Phys. Rev. D* 79 (2009) 055016
- [182] J. Erler, P. Langacker, S. Munir and E. Rojas, *JHEP* 0908 (2009) 017
- [183] Y. Li, F. Petriello and S. Quackenbush, *Phys. Rev. D* 80 (2009) 055018
- [184] J. Erler, P. Langacker, S. Munir and E. Rojas, *JHEP* 1111 (2011) 076
- [185] R. Diener, S. Godfrey and I. Turan, *Phys. Rev. D* 86 (2012) 115017
- [186] M. R. Buckley and M. J. Ramsey-Musolf, *Phys. Lett. B* 712 (2012) 261
- [187] M. Gonzalez-Alonso and M. J. Ramsey-Musolf, arXiv:1211.4581 [hep-ph]
- [188] P. Herczeg, *Phys. Rev. D* 68 (2003) 116004